

2**Three-Dimensional Kinematics
Underlying Gaze Control**

JOHN VAN OPSTAL

University of Nijmegen, Dept. of Medical Physics and Biophysics,
Geert Grooteplein 21, NL-6525 EZ Nijmegen, The Netherlands.

Tel.: (+31) 24 361 3834**Fax.: (+31) 24 354 1435****E-mail: johnvo@mbfys.kun.nl****Web: <http://www.mbfys.kun.nl/mbfys/people/johnvo/>**

Version February 16, 1998

Submitted to Springer Verlag,

E. Domany, J.L. Van Hemmen, and K. Schulten (eds),

Models of Neural Networks IV.

2

Three-Dimensional Kinematics Underlying Gaze Control

John Van Opstal¹

with 13 figures

Synopsis. The geometrical arrangement of the extra-ocular muscles enables rotations of the eyes in three dimensions (3D). It was already noted by Helmholtz [27] that the oculomotor system should therefore account for the non-commutative properties of 3D rotations. This principle entails that, in a series of rotations, the final orientation of the eye depends on the order in which they are generated.

As a consequence, this property could jeopardize the stability of the perceived visual world and greatly complicate visuomotor control. However, for head-fixed saccadic eye movements the problem is elegantly circumvented by Listing's law, which imposes precise geometric constraints on the ocular rotation axis. Recent findings have shown that somewhat different constraints, described by Donders' law, apply to conditions where both the eye and head are free to move.

A current controversy is whether these constraints are due to a non-commutative neural control strategy [47], or whether they result mainly from passive mechanical properties of the motor plants in combination with commutative neural controllers [52].

In this paper, we review the 3D kinematic principles of rotations that underlie the control of saccadic gaze shifts. We will argue that the experimental evidence strongly supports the notion that both Donders' and Listing's law have a major neural component.

2.1 Introduction.

Due to the highly inhomogeneous distribution of photo receptors on the retina, optimal visual resolution is only achieved for targets projected on the central retina (the fovea). In primates, the fovea has an effective diameter of less than a degree. Therefore, whenever the primate visual system decides to further explore the details of a peripheral visual target, the current gaze line must be precisely redirected at the object. Such a gaze shift is generated by the saccadic gaze control system. The saccadic orienting response is extremely rapid (peak velocities in monkey may exceed 1000 deg/s) and

¹Department of Medical Physics and Biophysics, University of Nijmegen, Geert Grooteplein 21, NL-6525 EZ, Nijmegen, The Netherlands.
E-mail: johnvo@mbfys.kun.nl Web: <http://www.mbfys.kun.nl/mbfys/people/johnvo/>

flexible, since in general, goal-directed gaze shifts may be achieved by an eye movement only, or by a myriad of different combinations of eye-, head-, and body rotations. Because of its clear function and apparent simplicity, the gaze control system has been studied extensively in many laboratories over the past two decades, and experimental data have been accounted for by an increasing number of detailed quantitative models.

Well into the seventies and early eighties, most studies were confined to gaze shifts in one dimension (1D; typically horizontal). Initially, recordings were made of head-fixed ocular saccades only, but later also horizontal head-movements were incorporated in these early studies [1,23].

Additional new insights into the saccadic system emerged when movements were recorded with two degrees of freedom (2D; horizontal and vertical) [22,48,67]. In recent years, however, the study of the gaze control system has been further extended to incorporate all three dimensions simultaneously (3D; horizontal, vertical, and torsional), and allowing for both the eye(s) (e.g. [13,32,43,60,70]) and head [20,58,65] to move freely. This paper will be specifically concerned with the concepts and results from these 3D studies².

2.2 The gaze control system in one and two dimensions.

The two important concepts that have dominated the visuomotor literature, and that are important for the present discussion, are the notions of *internal feedback* and *velocity integration*.

Internal feedback in saccade programming: When a visual stimulus is presented on the peripheral retina, the saccadic system might program an accurate eye movement to foveate the target, solely on the basis of the retinal error signal (defined as the difference between the current gaze direction and the desired gaze direction). Based on the following considerations, however, the retinal error, although sufficient at first glance, is not the only source of information on which the saccadic programmer relies:

- Saccades accurately compensate for any intervening eye movement that may occur between target presentation and saccade initiation. For example, in a flashed double-step paradigm, the subject has to generate saccades to two, briefly flashed targets, both extinguished well before the first movement onset. Despite the absence of visual feedback, the two saccades accurately land on both targets. A second saccade is even accurate when the second target is flashed *during* the first saccade (e.g. [24]).

²An excellent and nontechnical state-of-the-art review of the topics covered in this paper, and more, is provided in the proceedings of a recent workshop on 3D eye-, head-, and limb movements, held in Tübingen, Germany, 1995 [15].

- Monkeys can generate an accurate eye movement to an extinguished flashed target in darkness, even after the eyes had been driven away from their initial position, within the reaction time period, by electrical stimulation of the midbrain superior colliculus (SC; [42]).
- Accurate saccades can be generated to auditory targets in darkness, although the acoustic frame of reference is head-centered, rather than eye-centered (e.g. [17]). For this, the saccadic system needs to know the absolute position of the eyes in the orbit.

Internal feedback in saccade generation. It was further noted by Robinson and colleagues [50,66] that visual feedback is far too slow to be of any use for the accurate control of rapid eye movements (visual delays are in the same order of magnitude as typical saccade durations, roughly 50-60 ms). Since normal saccades have quite stereotyped kinematics with relatively little scatter, the possibility exists that they are generated by a preprogrammed pattern generator in the brainstem. However, without going into the details, strong additional evidence supports the idea that also the brainstem saccade generator is controlled by internal feedback:

- Saccades remain accurate despite a considerable, e.g. drug-induced or fatigue-related, variability in their kinematics (see [39]).
- Saccades that have been interrupted in midflight (by brief electrical microstimulation of the saccade gating system, embodied by the brainstem omnipause neurons (OPNs, [40]), and the rostral SC [46]) accurately re-acquire the target in complete darkness.

Velocity integration: The motoneuron signal that innervates the horizontal extraocular muscles is well characterized by a pulse-step activity pattern. The pulse is an intensive, phasic burst of action potentials, and is derived from so-called short-lead burst neurons in the paramedian pontine reticular formation [66]. The output of these latter neurons, $b(t)$, correlates well with a linear combination of instantaneous eye velocity, $\dot{e}(t)$, and acceleration, $\ddot{e}(t)$, and is needed to rapidly accelerate the plant against the viscous drag of surrounding tissues [66]. These premotor neurons are considered to embody the horizontal saccade generator, since lesions in this area completely, and specifically, abolish the occurrence of horizontal saccades [28].

The static elastic forces of the muscles are overcome by an eye-position related tonic innervation (the step). It was proposed by Robinson that such a signal could be obtained from the burst neurons by time-integrating the phasic burst [50,66]:

$$n(t) = \int_{t_0}^{t_1} b(t) \cdot dt + n(t_0) \cdot \exp(-t/T) \quad (1)$$

The existence of such a neural integrator stage has been convincingly confirmed by lesion studies of the nucleus prepositus hypoglossi (NPH) and

the medial vestibular nuclei (MVN). Under normal conditions, the neural integrator (NI) has a time constant of about $T=20$ s; lesions in this area, however, cause the time constant for horizontal fixations to drop well below 1 s [4].

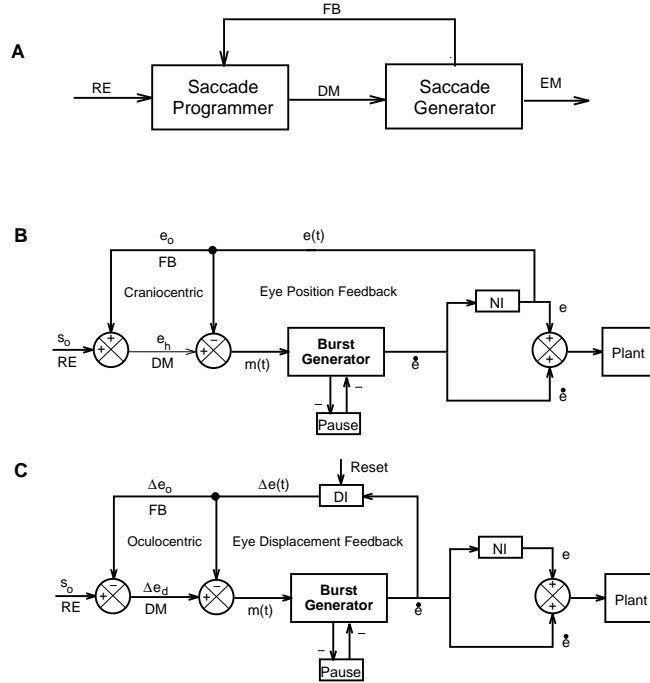


Fig. 1: (A) Overall organization of the saccadic system. The saccade programmer issues a desired movement command (DM) to the brainstem saccade generator. The programmer may update DM on the basis of feedback (FB) about intervening eye movements (EM). Also the generator is driven by local feedback (not shown). RE: retinal error. (B) In Robinson's eye position feedback model [50], the desired movement command is eye position in the head (e_h). Feedback from the neural integrator (NI) about initial (e_o) and current absolute eye position ($e(t)$) is provided to the programmer and the generator. The timing of the latter is controlled by an inhibitory gating mechanism embodied by pause neurons. s_o : retinal error; $m(t)$: current motor error; \dot{e} : eye velocity. (C) Eye displacement feedback model of Jürgens et al. [39]. The eye displacement signal (initial: Δe_o , current: $\Delta e(t)$) is computed by a resettable displacement integrator (DI).

A problem with the position feedback model, however, was the lack of evidence for a neural representation of e_h . In addition, the model did not provide a role for the SC, which was generally held to be part of a crucial stage in saccade visuomotor programming, since it provides direct input to the burst cells. Yet the neurophysiological evidence has indicated that the

SC rather seemed to encode a desired static displacement signal for the eyes, Δe_d , irrespective of initial eye position [49].

The 1D oculomotor plant. In models of the saccadic system (Fig. 1B,C), the brainstem pulse-step signal matches the dynamics of the horizontal plant. This is achieved by letting the net innervation of the oculomotor neurons, given by a linearly weighted sum of the NI ($n(t)$) and burst-cell outputs ($b(t)$), precisely counteract the muscle stiffness, K , tissue viscosity, V , and plant inertia, J , respectively. That is, if the pulse-step motoneuron innervation, $MN(t)$, is given by:

$$MN(t) = C \cdot n(t) + D \cdot b(t) \quad (2)$$

with C and D representing an internal model (as neural weights) of the plant's dynamics, then the actual eye velocity of the system is given by:

$$\dot{e}(t) = \frac{1}{V} \cdot [MN(t) - K \cdot e(t) - J \cdot \ddot{e}(t)] \quad (3)$$

For the system to have matched dynamics, it follows that $n=(K/C)e$, and $b=(1/D)(V\dot{e} + J\ddot{e})$, respectively. When the inertia of the globe may be ignored ($J \approx 0$), the burst neurons simply encode eye velocity according to $b=(V/D)\dot{e}$.

One-dimensional models. Since visual feedback plays no role in the experimental observations described above, it was hypothesized by Robinson that the saccade generator is driven by an internal feedback circuit in which a desired eye movement (issued by the saccade programmer) is continuously compared with an efference copy of the actual movement [50,66].

In the current literature there is some controversy on the nature of the signals involved in the different feedback mechanisms. In Robinson's original local feedback model [50], the saccadic burst generator is supposed to be driven by a neural estimate of the dynamic motor error, $m(t)$, by subtracting the desired eye position in the head, e_h , from an efference copy of current eye position, $e(t)$:

$$m(t) = e_h - e(t) \quad (4)$$

The latter signal is derived from the position neural integrator (NI, see Eq. (1); Fig. 1B). The former signal was obtained, in the model, by adding the retinal error of the target, s_o , with a neural estimate of the initial eye position, e_o (sampled from the initial state of the NI, $n(t_o)$):

$$e_h = s_o + e_o \quad (5)$$

Therefore, recent displacement feedback models proposed that the dynamic motor error is obtained by comparing the collicular signal with an efference copy of actual eye *displacement* (e.g. [39]; Fig. 1C):

$$m(t) = \Delta e_d - \Delta e(t) \quad (6)$$

The latter signal is produced by a feedback resettable displacement integrator (DI), which integrates eye velocity, just like the position NI, but needs to be reset to zero after each saccade. To account for the double-step results, and the inter-saccadic eye-displacement experiments (see above), the former signal was not directly taken as the initial retinal error of the target, s_o , but was assumed to take the displacement of the previous saccade, Δe_o , into account, by ‘*remapping*’ the target into oculocentric coordinates:

$$\Delta e_d = s_o - \Delta e_o \quad (7)$$

Although the revised model solved one problem (it accommodated the SC), it created a new one (lack of neurophysiological support for a DI).

Two-dimensional ocular control: The vertical saccadic pulse-step generator in the brainstem consists of short-lead burst cells in the rostral interstitial nucleus of the medial longitudinal fasciculus (riMLF) [29], and the neural integrator in the interstitial nucleus of Cajal (iC) [9]. Neurophysiology has revealed that cells in this burst generator are actually tuned to movements in the vertical/torsional plane ([32] for review, and [8,9]).

Both saccade generators receive a common input command from the SC, that represents a desired displacement of the eye (Δe_d) relative to the initial eye position (see also above). The SC signal is spatially encoded in a topographic motor map, in the sense that neighbouring recruited regions encode similar saccade vectors by their *location* within the map, rather than by the intensity of the neural activity (e.g. [33,49,70]). The transformation of this oculocentric *vectorial* signal into the appropriate innervation patterns of the extraocular muscles, has become known as the *spatial-temporal* transformation stage, and involves two different processes:

- (a) Vector decomposition (VD) into the horizontal and vertical saccade components.
- (b) Pulse generation (PG) of motor error, $m(t)$, into an eye velocity command, $\dot{e}(t)$.

Because the latter stage is assumed to be nonlinear (described by a saturating function that accounts for the observed saccade kinematics: $\dot{e} = a[1 - \exp(-b \cdot m)]$; [50,66,67]), the order in which these two processes are implemented matters (it is a non-commutative operation: $VD \cdot PG \neq PG \cdot VD$).

An interesting question therefore is, whether the horizontal and vertical components of an oblique saccade are generated by independent pulse generators, or whether they are somehow coupled.

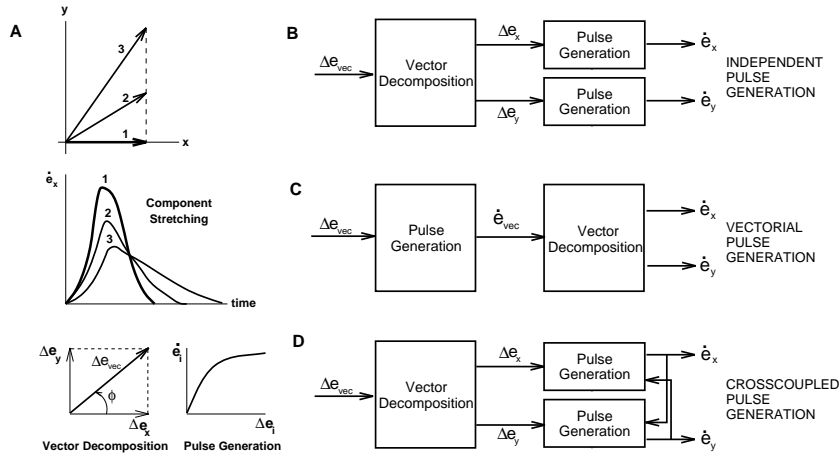


Fig. 2: Two-dimensional extensions of the saccadic system should account for the fact that oblique saccades are approximately straight, and that the peak velocity and duration of horizontal and vertical saccade components systematically depend on saccade direction, ϕ ('stretching') (A). Note that the order of the vector decomposition (linear) and pulse generation (nonlinear) processes matters. (B) In the Independent model, vector decomposition precedes pulse generation. This model therefore predicts that component velocity is independent of saccade direction (no stretching). (C) In the Common Source scheme, a vectorial pulse generator precedes the decomposition of the vectorial eye velocity signal. (D) The Crosscoupling scheme resembles the Independent model, but the pulse generators are mutually coupled. The latter two models produce both stretching and straight saccades.

A detailed behavioural and model study of monkey oblique saccades revealed that both saccade components are tightly synchronized and coupled, such that approximately straight saccades are elicited in all directions [67]. For example, the kinematics of a fixed horizontal component, when compared for a set of oblique saccades in different directions (having different vectorial amplitudes and vertical components), systematically depend on the direction of the saccade vector. The peak velocity of the horizontal component decreases as function of the angle with the horizontal meridian, such that its duration closely matches the duration of the vertical component (Fig. 2A). The vertical component is subjected to similar effects. In this way, a given component always reaches its highest peak velocity when executed in isolation (either purely horizontal (nr. 1 in Fig. 2A), or purely vertical movements). The reduction in peak velocity, and concomitant increase in component duration, has been termed *component stretching* [48,67]. It is generally believed that this phenomenon reflects a property of the neural organization of the saccade generator.

Although this finding excludes an independent control of the horizontal and vertical burst generators (Fig. 2B), two conceptually different schemes

coexist that both account for these findings (see Fig. 2C,D). In the ‘*cross-coupling scheme*’ (Fig. 2D), the horizontal and vertical burst-generators receive a decomposed horizontal/vertical motor error input from the SC, like in the independent scheme, but mutually couple their velocity outputs at the brainstem level [48]. In contrast, in the so-called ‘*common source scheme*’ (Fig. 2C) a vectorial burst generator issues a vectorially-encoded pulse command, that is subsequently decomposed into the respective horizontal and vertical velocity components [67]. Note, that straight saccades and stretching are emergent properties of this latter model, whereas they are a specific design feature in the crosscoupling model.

Eye-head movement control in 1D and 2D: When the head is also allowed to move, the position of the eye in space (gaze in space, g_s) now comprises both the position of the eye in the head, e_h , and the position of the head in space, h_s , according to:

$$g_s = e_h + h_s \quad (8)$$

The nature of combined horizontal eye-head movements has been studied extensively in human, cat and monkey (e.g. [1,23,51]). Initially, Bizzi and colleagues proposed that head-free gaze saccades are, like head-fixed gaze saccades, programmed as an ocular saccade, independent of the occurrence and size of a concomitant head movement. According to this so-called *oculocentric hypothesis*, the vestibulo-ocular reflex (VOR) would cancel any contribution of the head to the gaze shift by causing the eyes to counter-rotate by the same amount [1].

Despite its simplicity, a serious flaw of this model is that such a system would not enable accurate gaze shifts beyond the oculomotor range. In addition, several experiments have shown that the action of the VOR is actually suppressed during gaze saccades. These and other observations have led to the conclusion that the oculocentric hypothesis is strictly valid only for gaze shifts smaller than ~ 10 deg.

As an alternative for the oculocentric hypothesis, the conceptual oculomotor model (see above) was extended to a gaze control model in the head-free condition [23]. According to this *gaze feedback hypothesis*, an internally created, instantaneous gaze motor-error (i.e. desired gaze \sim minus current gaze displacement) is used to drive the oculomotor system. In this way, the accuracy of gaze saccades can be maintained, regardless of head movements, even if the VOR is suppressed during the movement.

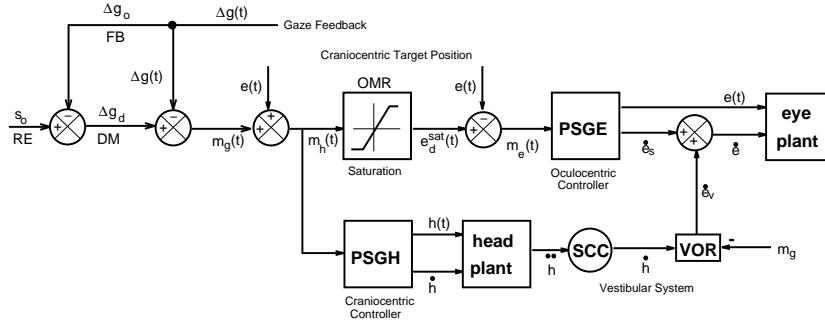


Fig. 3: Two-dimensional eye-head coordination model, adapted from [22]. Eye and head are driven by a desired gaze displacement signal, Δg_d (emanating from the SC) that is updated by feedback about current gaze displacement, $\Delta g(t)$. Note, that this part of the model could alternatively be formulated in terms of a desired gaze-position signal in space (see e.g. Fig. 13). The head is driven by a current head motor-error signal, $m_h(t)$. The same signal is also fed into a 2D neural representation of the (circular) oculomotor range (OMR) to determine the desired position of the eye in the head, e_d^{sat} . The eye pulse-step generator is then driven by instantaneous eye motor-error, $m_e(t)$ (cf. with Robinson’s model; for clarity, local feedback is omitted). The VOR is inhibited by the current gaze motor error signal, $m_g(t)$. As this signal falls to zero during the gaze shift (i.e. eye is on target), the VOR is re-activated by the ongoing head movement.

Note, that the concept of gaze feedback by itself does not specify the head motor command. It was initially proposed, on the basis of gaze control studies in the cat, that both the oculomotor system and the head motor system are controlled by the *same* internally created gaze motor-error signal [19]. Although several behavioural and neurophysiological studies seemed to provide support for this so-called *common gaze model*, a recent analysis of the eye-, head- and gaze trajectories in two dimensions rather suggested that the two motor systems are driven by signals expressed in their own frames of reference (oculocentric and craniocentric, respectively; [22]). For example, it was found that when eyes and head start from unaligned initial positions, both motor systems make a goal-directed saccade toward the target. Since eye and head then simultaneously move in quite different directions, they must be driven by different inputs. Fig. 3 presents a simplified scheme that summarizes the ideas of gaze feedback in combination with different eye- and head controllers. The scheme is qualitatively supported by recent data obtained from SC stimulation in the head-free monkey [16]. For specific details, the reader is referred to [22].

Although not detailed in Fig. 3, a complete model of the gaze control system should also incorporate the dynamics of the head motor system. In its simplest 1D form, the head is modeled by a linear, overdamped, second-order differential equation (e.g. [19], compare to Eq. (3)). In contrast

to the eye, the head inertia is substantial and should not be ignored. In addition, for head movements in non-horizontal directions, there may also be a considerable translational component to the movement, due to the flexibility of the neck vertebrae that cause the rotation axes of the head-neck system not to intersect in a single point. We will, however, not deal with the latter problem in this paper.

2.3 New aspects for eye rotations in 3D.

That the eye should be considered as a rigid sphere rotating about its head-fixed center [32] can be ignored as long as movements are confined to the horizontal plane (only rotation about a fixed, vertical axis, so that parametrization by a single scalar, the horizontal angle, suffices). As soon as movements are allowed in more dimensions, however, the ocular rotation axes may differ from saccade to saccade, and a full 3D approach is called for.

The three antagonistic pairs of extra-ocular muscles pull in approximately orthogonal directions, so that movements of the eye are in principle allowed three independent degrees of freedom [3]: the horizontal recti (LR and MR) rotate the eye about a vertical axis (\mathbf{z}) to generate horizontal gaze shifts, whereas the vertical recti (SR, IR) and oblique muscles (SO, IO) define two orthogonal rotation axes in the vertical-torsional ($\mathbf{y-x}$) plane (Fig. 4).

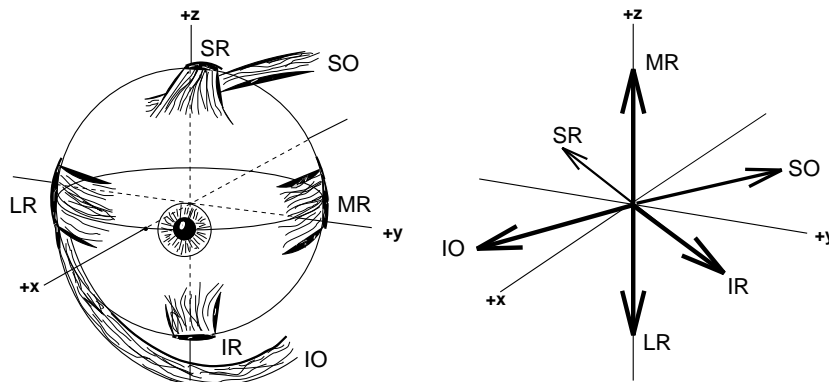


Fig. 4: Left: frontal view of the right eye's six extraocular muscles, shown with the eye rotated about 20 deg leftward from the primary direction ($+\mathbf{x}$). Right: Schematic of the muscle rotation axes, represented in the head-fixed, primary coordinate system, $(\mathbf{x}, \mathbf{y}, \mathbf{z})$. Note that the antagonist pairs (LR-MR, SR-IR, and SO-IO) pull in three, approximately orthogonal directions. The torque vectors are also approximately aligned with the on-directions of the semicircular canals.

Despite the apparent simplicity of the mechanical organization of the oculomotor system, it also induces an interesting problem that was already

noted more than a century ago by Helmholtz [27] and has received renewed attention in more recent studies [14,26,30,52,60,70,77].

The problem arises because 3D rotations of rigid bodies are *non-commutative*. As a consequence, the order in which two consecutive rotations about different axes are performed, determines the final orientation of the object [21]. The problem is absent as long as movements are constrained to one dimension only, and because of this, it has been ignored in oculomotor studies for a long time. Yet, it has been recognized that this property could have important consequences for the way in which eye (and head) movements are programmed and generated [32,60,62].

If gaze shifts would be controlled without accounting for the noncommutativity of 3D rotations, problems could arise for the visual perceptual system, for visuomotor control, as well as for the motor system proper.

First, the orientation on the retina of fixed objects in the visual world would depend on the history of previous eye rotations. Since typically about three saccades per second are generated in all directions and from all possible initial eye positions, the ability to perceive a stable visual world, and to precisely control binocular alignment for adequate depth perception, would be seriously challenged.

Second, the visual information on the retina is, by itself, not sufficient to produce accurate eye movements (see also below). The absolute position of the eye in the head should be incorporated to prevent systematic mislocalizations of the stimulus, especially for targets presented in the retinal periphery with eccentric initial eye positions, or with considerable torsion [7,10,60]. Finally, also from the motor point of view, problems could arise if the motoneuron signals to the plant would not account for the nonabelian property. However, as will be discussed below, a precise assessment of this problem requires a detailed model of the plant dynamics.

Fig. 5 illustrates the problem for the vestibulo-ocular reflex (VOR) by letting the eye maintain fixation of a stationary point in space after two different sequences of head rotations. Obviously, a properly functioning VOR requires that the amount of head rotation is exactly canceled by an equal and opposite rotation of the eyes in the head. Like for the saccadic system, it is generally accepted that the vestibular input, which at the level of the vestibular afferents is proportional to head angular velocity, is neurally integrated (by the *same* NI as in Fig. 1B) to generate the tonic eye position signal. However, as was pointed out by Tweed and Vilis [60], in 3D, eye position is *not* obtained by taking the time-integral of eye angular velocity.

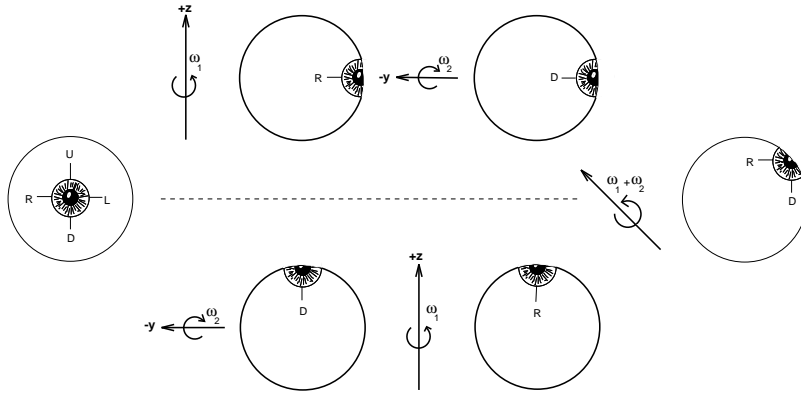


Fig. 5: Noncommutativity of rotations illustrated for a perfectly functioning VOR that compensates for two consecutive 90 deg head rotations about the head-fixed $-z$ (rightward head movement) and $+y$ (downward) axes, respectively (top). The orientation of the eye in the head is shown (as if viewing onto the subject's nose). Reversing the order of the two head-rotations (bottom) yields very different final eye positions, although the total amount of rotation is equal for the two cases. This property results from the fact that eye position is not the integral of eye angular velocity. Rotation about an axis that is the vectorial sum of the (simultaneously presented) angular velocity signals (center, right) yields yet a different eye position without torsion. After [59].

The two exaggerated examples in Fig. 5 clearly illustrate that the VOR brings the eyes in very different positions in the head (to the extreme left and with 90 deg counterclockwise torsion for the first series of head rotations, but upward and 90 deg clockwise torsion for the second example). Yet, it is also obvious that the total time integral of the two consecutive angular velocity signals for both cases (cf. $\int(\omega_1 + \omega_2) dt$ vs. $\int(\omega_2 + \omega_1) dt$), is identical ($\pi/2(\mathbf{e}_y - \mathbf{e}_z)$). Thus, if the tonic oculomotor neuron firing would be produced by a neural integrator that receives eye angular velocity as an input, the eyes would have ended up in identical, but wrong, positions [59,60].

Clearly, these problems do not seem manifest in actual visuomotor behaviour (we do have a stable visual percept despite eye movements, our eye muscles do not knot, and the VOR works appropriately, also in 3D), so the question is what features of the oculomotor and eye-head control systems resolve these potential problems.

It is important to stress at this point, that the logic of this example does not depend on any mechanical plant model. It is only assumed that identical oculomotor neuron firing patterns (regardless their origin) lead to identical eye positions in the head. The principles of noncommutative rotational kinematics therefore require that the central nervous system somehow takes the integrator problem of Fig. 5 into account. Since the neural integrator is thought to be shared by all oculomotor subsystems (not only the VOR,

but also by the pursuit, the saccadic, and vergence systems), this problem affects the cornerstone of gaze control theories [30,60,62].

To successfully deal with the underlying concepts in a quantitative way, however, one has to apply the mathematical framework of 3D rotational kinematics. The main principles, deemed relevant for the eye-head gaze control system, will therefore be briefly introduced. Some of the computational details, when not immediately needed for comprehending the line of thought, have been delegated to the Appendix.

2.4 Mathematics of 3D rotational kinematics.

Any finite rotation of a rigid body can be fully described by a real, orthogonal, proper 3×3 matrix (i.e. with determinant $+1$, and transpose $\mathbf{R}^T = \mathbf{R}^{-1}$), and all 3D rotations make up the special, nonabelian (i.e. noncommutative), orthogonal group $\text{SO}(3)$ [57].

There are many ways to describe the orientation of a rigid body. Here, we will not review all the different methods (like rotation matrices, and the twelve different sets of Euler angles, see e.g. Goldstein [21] for a detailed treatment). Rather, we will present those parametrizations that have been particularly useful in their applications to the oculomotor and eye-head control systems. We start out with the basic equation describing the rotation of an arbitrary vector, and then proceed with the framework of quaternions and the Euler-Rodrigues coordinates.

2.4.1 Finite rotations

According to Euler's theorem, the general displacement of a rigid body, when one point of the body remains fixed in space, is uniquely described by a single-axis rotation, with the rotation axis passing through the fixed point [21].

To describe eye orientations in 3D, we adopt a right-handed, head-fixed cartesian coordinate system (like in Fig. 4), with the origin in the center of the eye. The $\hat{\mathbf{e}}_x$ -axis points forward (clockwise torsional rotations positive), the $\hat{\mathbf{e}}_y$ -axis lies along the interocular line connecting the two centers (downward rotations positive), and the $\hat{\mathbf{e}}_z$ -axis points upward (leftward rotations positive).

The fixed-axis rotation of an arbitrary vector, \mathbf{u} , over some finite angle, ρ (in radians), around axis $\hat{\mathbf{n}}$ (a unit vector, see Fig. 6), is then given by:

$$R(\hat{\mathbf{n}}, \rho) \mathbf{u} = (\mathbf{u} \bullet \hat{\mathbf{n}})\hat{\mathbf{n}} + \sin(\rho)(\hat{\mathbf{n}} \times \mathbf{u}) - \cos(\rho)\hat{\mathbf{n}} \times (\hat{\mathbf{n}} \times \mathbf{u}) \quad (9)$$

in which \bullet is the scalar (dot) product, and \times the vector (cross) product.

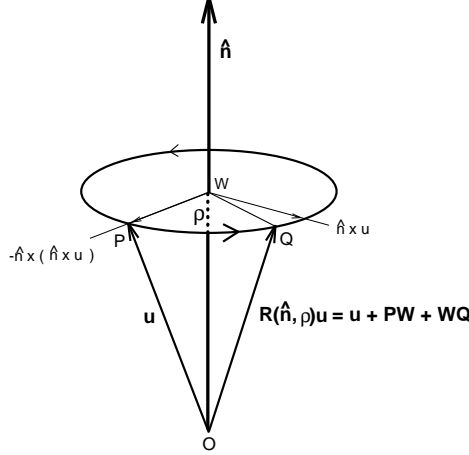


Fig. 6: Rotation of vector \mathbf{u} over finite angle ρ about axis $\hat{\mathbf{n}}$.

Note that $\mathbf{u} = (\mathbf{u} \bullet \hat{\mathbf{n}})\hat{\mathbf{n}} - \hat{\mathbf{n}} \times (\hat{\mathbf{n}} \times \mathbf{u})$, from which a Taylor expansion yields in good approximation:

$$R(\hat{\mathbf{n}}, \rho) \mathbf{u} = \mathbf{u} + \rho \hat{\mathbf{n}} \times \mathbf{u} + \frac{1}{2} \rho^2 \hat{\mathbf{n}} \times (\hat{\mathbf{n}} \times \mathbf{u}) + \mathcal{O}(\rho^3) \quad (10)$$

For fixed-axis rotations, only the angle ρ is a function of time, and thus $R = R(\hat{\mathbf{n}}, \rho(t)) = R(t)$. The angular velocity, $\omega(t)$, with which \mathbf{u} spins around the rotation axis $\hat{\mathbf{n}}$ is a vector defined by

$$\omega(t) \equiv \dot{\rho}(t) \hat{\mathbf{n}} \quad (11)$$

($\dot{\rho}$ is the time derivative of ρ). The angular velocity is related to the rotation $R(t)\mathbf{u}$ by the well-known kinematic relation:

$$\begin{aligned} \dot{R}(t)\mathbf{u} &= \omega(t) \times R(t)\mathbf{u} \\ &\approx \dot{\rho}(t) [\hat{\mathbf{n}} \times \mathbf{u} + \rho ((\hat{\mathbf{n}} \bullet \mathbf{u})\hat{\mathbf{n}} - \mathbf{u})] \end{aligned} \quad (12)$$

where we have used Eq. (10) and Eq. (11). Here, $\dot{R}(t)\mathbf{u}$ will be designated the *coordinate velocity* vector. It is the velocity with which the tip of \mathbf{u} rotates around the axis. Note from Fig. 6 and Eq. (12), that for a given angular velocity, the coordinate velocity vector depends on both the orientation of \mathbf{u} re. the rotation axis, and on its length.

An important question for understanding 3D gaze control, briefly touched upon in the discussion of Fig. 5, is whether the saccadic short-lead burst neurons in the brainstem encode a coordinate velocity or an angular velocity signal. As will become clear below, the distinction has important implications for the neural organization of the saccadic system, and for its interactions with other oculomotor subsystems (like the vestibular system, the smooth pursuit system, and the vergence system). Before elaborating

further on these matters, we will first provide an outline of the mathematical framework within which these concepts can be elegantly represented. For a more detailed treatment, the reader is referred to [2,57].

2.4.2 Quaternions.

W.R. Hamilton (1843) was the first to propose a closed algebraic framework for the multiplication of 3D vectors. The result of his work was that such an algebra had to be described by hypercomplex, four-dimensional entities, which he named quaternions [2]. Quaternions have a particularly useful and natural relationship with fixed-axis rotations and it is for that reason that their properties will be reviewed in somewhat more detail in this section. A quaternion is written as a four-component complex quantity defined by:

$$q \equiv q_o + \mathbf{I} \bullet \mathbf{q} \quad (13)$$

with $\{q_o, q_x, q_y, q_z\} \in \mathcal{R}$, the four quaternion components (q_o is called the scalar part of the quaternion, $S(q)$, and $\mathbf{q} = (q_x, q_y, q_z)$ is its vector part, $V(q)$). The *adjunct* (or complex conjugate) of the quaternion is given by $q^* = q_o - \mathbf{q} \bullet \mathbf{I}$. The components of the complex vector, $\mathbf{I} = (i, j, k) \in \mathcal{C}$ obey the following noncommutative, cyclic relations³:

$$i^2 = j^2 = k^2 = i \cdot j \cdot k = -1 \quad (14)$$

$$i \cdot j = -j \cdot i = k \quad j \cdot k = -k \cdot j = i \quad k \cdot i = -i \cdot k = j$$

Main properties of quaternions. Armed with these definitions, it is now possible to multiply two arbitrary quaternions, say $p = p_o + \mathbf{p} \bullet \mathbf{I}$ and $q = q_o + \mathbf{q} \bullet \mathbf{I}$. Applying Eq. (13) and Eq. (14), the following important rule for the quaternion product is obtained:

$$pq = p_o q_o - \mathbf{p} \bullet \mathbf{q} + (p_o \mathbf{q} + q_o \mathbf{p} + \mathbf{p} \times \mathbf{q}) \bullet \mathbf{I} \quad (15)$$

Thus, multiplication of two quaternions results in a new quaternion (hence, they form a closed algebraic system). Note that, in general, the vector part of the product quaternion, $V(pq)$, does not lie in the plane spanned by \mathbf{p} and \mathbf{q} . More importantly, however, $pq \neq qp$ whenever \mathbf{p} and \mathbf{q} are not parallel (or zero). This latter property, the noncommutativity of quaternion multiplication, is deeply connected (see below) to the noncommutativity of rotational kinematics briefly outlined above.

³It can be readily verified that the properties of the components of the complex vector \mathbf{I} can be identified with the Pauli spin matrices $[\sigma_i]$ which are the generators of the SU(2) group (the special group of complex, hermitean 2x2 unitary matrices; see e.g. [21,57]):

$$[\sigma]_o = \begin{pmatrix} 1 & 0 \\ 0 & 1 \end{pmatrix}, \quad [\sigma]_1 = \begin{pmatrix} 0 & 1 \\ 1 & 0 \end{pmatrix}, \quad [\sigma]_2 = \begin{pmatrix} 0 & -i \\ i & 0 \end{pmatrix}, \quad [\sigma]_3 = \begin{pmatrix} 1 & 0 \\ 0 & -1 \end{pmatrix},$$

which establishes the local isomorphism between SO(3) and SU(2) ($1 \Leftrightarrow [\sigma_o]$, $i \Leftrightarrow [\sigma_1]$, $j \Leftrightarrow [\sigma_2]$, $k \Leftrightarrow [\sigma_3]$).

The length (or norm) of a quaternion is given by

$$|q| \equiv \sqrt{qq^*} = \sqrt{q_o^2 + \mathbf{q} \bullet \mathbf{q}} \quad (16)$$

Taken together, Eq. (13) can be parametrized, for reasons that will become clear below, by;

$$q = |q| \cdot (\cos(\theta) + \sin(\theta) \cdot \hat{\mathbf{e}} \bullet \mathbf{I}) \quad (17)$$

Here, $\hat{\mathbf{e}}$ denotes the unit vector (or axis) of the quaternion, with $e_i = q_i / \sqrt{q_x^2 + q_y^2 + q_z^2}$, and θ is the quaternion angle ($\cos(\theta) = q_o / |q|$).

Note that in this framework, a 3D vector can be regarded as a quaternion with scalar part zero, any real number is a quaternion with vector part zero, and any complex number is a quaternion with vector components $(q_y, q_z) = 0$. The *inverse* of a quaternion is obtained by the demand $qq^{-1} = q^{-1}q = 1$, and it can be readily verified from Eq. (15), Eq. (16), and Eq. (17) that it is determined by⁴:

$$q^{-1} = \frac{1}{|q|} \cdot (\cos(\theta) - \sin(\theta) \cdot \hat{\mathbf{e}} \bullet \mathbf{I}) = \frac{q^*}{|q|^2} \quad (18)$$

Relation with fixed-axis rotations. Now what is the relation between a quaternion, q , and the rotation of an arbitrary vector, \mathbf{u} , about an axis, $\hat{\mathbf{n}}$, over angle ρ (see above)? An elegant theorem that follows from the rules of quaternion calculus, described above, says that if one parametrizes a quaternion by Eq. (17), then the new vector \mathbf{u}' :

$$\mathbf{u}' = q\mathbf{u}q^{-1} = R(\hat{\mathbf{n}}, 2\theta) \mathbf{u} \quad (19)$$

In other words, the unit vector, $\hat{\mathbf{e}}$, of the quaternion is directed along the rotation axis $\hat{\mathbf{n}}$, and vector \mathbf{u} is rotated by twice the quaternion angle around this axis. This important property may be verified in Appendix A-1.

Without loss of generality, it is customary to constrain the norm $|q| = 1$, so that the following unit quaternion fully parametrizes the rotation of an arbitrary vector about $\hat{\mathbf{n}}$ over angle ρ :

$$q = \cos(\rho/2) + \sin(\rho/2) (\hat{\mathbf{n}} \bullet \mathbf{I}) = \exp\left(\frac{\rho}{2} \cdot \hat{\mathbf{n}} \bullet \mathbf{I}\right) \quad (20)$$

Geometrically, there is an interesting correspondence between the space of unit quaternions, and the unit sphere in 3D cartesian space. In particular, the real quaternion $q = 1$ (i.e. $\theta = 0$) corresponds to any single point on the

⁴One may now also define the *quotient* of two quaternions, p and q , as the solution, r , of an equation of the following type: $p = qr$. However, rather than writing $r = p/q$ for the solution, one should distinguish the two different possibilities: $r_1 = pq^{-1}$, and $r_2 = q^{-1}p$, which are generally unequal due to the noncommutativity of quaternion multiplication. In this case, r_2 is the correct solution (left quotient), which was obtained by left-multiplying both sides with q^{-1} (the right quotient r_1 is the solution of $p = rq$).

unit sphere, whereas $q = -1$ (i.e. $\theta = \pi$) describes any great circle on the unit sphere (in both cases, $\hat{\mathbf{e}}$ is arbitrary). All other non-real quaternions (with $\theta \in (0, \pi)$) correspond to arcs (of length θ radians) that are part of the great circle perpendicular to the quaternion (or polar) axis $\hat{\mathbf{e}}$.

Angular and coordinate velocities in q representation. As was briefly mentioned in the introduction of this section, a proper understanding of 3D gaze control requires that a distinction be made between the angular and the coordinate velocity vectors. If a quaternion, q , may be identified with the rotation $R(\hat{\mathbf{n}}, \rho)\mathbf{u}$, then the time derivative of the quaternion, $\dot{q} = dq/dt$, corresponds to the coordinate velocity, Eq. (12), of the rotating vector.

In Appendix A-2, a derivation is given for the relation between the coordinate velocity, \dot{q} , and the angular velocity, ω , in the quaternion parametrization. The result is given by the following simple equation [60]:

$$\dot{q} = \frac{\omega q}{2} \quad (21)$$

By applying the product rule Eq. (15) for quaternions one finds immediately for the vector part of Eq. (21):

$$\dot{\mathbf{q}} = \frac{1}{2}(q_o\omega + \omega \times \mathbf{q}) \quad (22)$$

(note that $\omega_o = 0$) and, similarly, the reverse relation is obtained by right-multiplication of both sides in Eq. (21) with q^{-1} :

$$\omega = 2\dot{q}q^{-1} = 2(q_o\dot{\mathbf{q}} - \dot{q}_o\mathbf{q} + \mathbf{q} \times \dot{\mathbf{q}}) \quad (23)$$

It is now also possible to obtain the coordinate and angular acceleration of the body, by evaluating the time derivatives of Eq. (21) and Eq. (23). For example, for the coordinate acceleration one obtains:

$$\ddot{q} = \frac{1}{2}(\dot{\omega}q + \omega\dot{q}) \Rightarrow \ddot{\mathbf{q}} = \frac{1}{2}\left[q_o\dot{\omega} - \frac{\omega^2}{2}\mathbf{q} + \dot{\omega} \times \mathbf{q}\right] \quad (24)$$

2.4.3 Rotation vectors.

A slightly different parametrization of a 3D rotation is provided by the Euler-Rodrigues coordinates [41], designated in the oculomotor literature as the *rotation vector* representation. The rotation vector is introduced here because it has some interesting geometric properties for modeling the saccadic system. One such property is that saccades in Listing's plane, when viewed as fixed-axis rotations, follow straight lines (i.e. shortest paths, or geodesics) in rotation vector space (see [30], and below). The rotation vector, and its inverse, is defined by:

$$\mathbf{r} \equiv \tan(\rho/2)\hat{\mathbf{n}} \quad \text{and} \quad \mathbf{r}^{-1} = -\mathbf{r} \quad (25)$$

The correspondence between quaternions and rotation vectors is therefore established by:

$$\mathbf{r} = \frac{V(q)}{S(q)} = \frac{\mathbf{q}}{q_o} \quad (26)$$

Obviously, a potential disadvantage of the rotation vector representation emerges for very large angles: when $q_o \rightarrow 0$ (for $\rho \rightarrow 180$ deg) the length of the rotation vector rapidly approaches infinity, and is therefore ill-defined. For head-fixed saccades, however, rotation vectors are particularly useful parametrizations.

By applying Eq. (26) to the product of quaternions Eq. (15), a simple rule for rotation vector multiplication is derived that gives the combined result of rotation \mathbf{r}_1 , followed by a second rotation, \mathbf{r}_2 :

$$\mathbf{r}_2 \circ \mathbf{r}_1 = \frac{V(q_2 q_1)}{S(q_2 q_1)} = \frac{\mathbf{r}_1 + \mathbf{r}_2 + \mathbf{r}_2 \times \mathbf{r}_1}{1 - \mathbf{r}_1 \bullet \mathbf{r}_2} \approx \mathbf{r}_1 + \mathbf{r}_2 + \mathbf{r}_2 \times \mathbf{r}_1 \quad (27)$$

Here \circ denotes the product of rotation vectors, and the approximation holds up to $\mathcal{O}(\rho^3)$. Using Eq. (22) and Eq. (23), one can also find the equivalent relations for the angular and coordinate velocities in the rotation vector representation. The exact results are (see [30] and Appendix A-2):

$$\boldsymbol{\omega} = \frac{2(\dot{\mathbf{r}} + \mathbf{r} \times \dot{\mathbf{r}})}{1 + \mathbf{r} \bullet \mathbf{r}} \approx 2(\dot{\mathbf{r}} + \mathbf{r} \times \dot{\mathbf{r}}) \quad (28)$$

and, similarly, for the reverse relation:

$$\dot{\mathbf{r}} = \frac{1}{2}(\boldsymbol{\omega} + \boldsymbol{\omega} \times \mathbf{r} + (\boldsymbol{\omega} \bullet \mathbf{r})\mathbf{r}) \quad (29)$$

which may also be compared to Eq. (12).

2.5 Donders' law and Listing's law

Eye positions. In what follows, eye positions will be described by rotation vectors Eq. (25), the coordinates of which are expressed in the head-fixed primary frame of reference (for definition, see below). Conceptually, this means that any 3D eye position is parametrized by the *virtual* rotation that brings the eye from the center of the head-fixed cartesian coordinate system to the current position. The origin of the primary reference frame is, by definition, the zero position vector, $\mathbf{r} = \mathbf{0}$, and is called the *primary position* of the eye. It is important to note, that the primary position is a geometrical concept that is not necessarily equal, or even close to, the center of the oculomotor range.

A *secondary* eye position is obtained by a rotation from the primary position about either the horizontal or vertical axis of the primary coordinate system. For example, a position 20 deg to the left of primary position is described by the rotation vector $\mathbf{r} = (0, 0, 0.176)$ (positive rotation about

the vertical axis), where the units are measured in half-radians. As a rule of thumb, every 0.01 half-radian roughly corresponds to $2 \cdot \arctan(0.01) \approx 1$ deg rotation about the axis.

A *tertiary* position is any eye position that obeys Listing's law (see below) and is not a primary or secondary position. Eye positions that do not follow Listing's law Eq. (33) are called *quaternary* positions.

Donders' law. The fixation of a point target is a redundant motor task, since the direction of the target (for each eye) is fully determined by two coordinates (azimuth and elevation re. fovea). The amount of torsion about the visual axis remains unspecified by the task.

Donders [27,38] proposed, on the basis of retinal after-image experiments, that for each target position in 3D space the gaze direction determines a unique orientation of the eye, independent of the trajectory followed to get to that position. In other words, ocular torsion is fully specified by the horizontal and vertical components of the gaze direction. This important rule is known as Donders' law, and restricts eye positions to a two-dimensional (2D) subspace:

$$\mathbf{r}_x = \text{function}(\mathbf{r}_y, \mathbf{r}_z) \quad (30)$$

The precise geometry of this surface, however, is not specified by Donders' law and, as will be seen below, appears to depend on the gaze orienting task. Since ocular torsion is constrained by a smooth function, Donders' law elegantly solves the problem of accumulation of torsion: whatever the path followed by the eyes, torsion remains on the surface defined by Eq. (30). An illustrative example of a Donders' surface is provided by a gimbal system. In a gimbal system, a 3D orientation is described by three consecutive rotations about a nested set of axes. In physics, the Euler angles constitute such a gimbal system, and in fact, twelve different types of gimbals can be constructed to achieve the same objective [21].

In the so-called *Fick gimbal*, which will be relevant in the discussion of 3D eye-head coordination (see below), the orientation of the rotating body is described by making first a horizontal rotation about the *space-fixed* vertical axis ($\hat{\mathbf{e}}_z$, angle θ_F). Then, a second, vertical, rotation is performed about the new *body-fixed* horizontal axis ($\hat{\mathbf{e}}'_y$, angle φ_F), which has been rotated away from the space-fixed coordinate system by the first rotation. Finally, a third rotation is performed about the new, body-fixed frontal axis, ($\hat{\mathbf{e}}''_x$, angle ψ_F), inducing torsion. Rotations about body-fixed axes are known as *passive* rotations, since they involve a rotation of the coordinate system. In contrast, *active* rotations are about space-fixed axes, and generate the actual rotation of the body [21].

Suppose that gaze positions would somehow be generated by such a gimbal system. Then, if gaze would adhere to Donders' law Eq. (30), its torsional component is determined by the horizontal (head-fixed) and vertical (eye-fixed) rotation angles only (θ_F and φ_F , respectively), i.e. a reduced, two-axis

system; cf. Fig. 5). The resultant position of gaze is then computed as follows:

$$\begin{aligned} \mathbf{r}_F &= \mathbf{r}'_{eye} \circ \mathbf{r}_{head} = (\mathbf{r}_{head} \circ \mathbf{r}_{eye} \circ \mathbf{r}_{head}^{-1}) \circ \mathbf{r}_{head} = \mathbf{r}_{head} \circ \mathbf{r}_{eye} \\ &= [-\tan(\theta_F/2) \cdot \tan(\varphi_F/2), \tan(\varphi_F/2), \tan(\theta_F/2)] \end{aligned} \quad (31)$$

Note, that the passive rotation of the horizontal axis can be transformed into an active vertical rotation of the eye (in head-fixed coordinates), by reversing the order of the horizontal and vertical rotations (e.g. [21,25,57]). Figure 7 illustrates the 3D ‘Fick’ trajectories in rotation-vector space, when the eye first goes to target A from the primary position, $\mathbf{r} = \mathbf{0}$, in two steps (PQA), and then tracks a square array of targets in the clockwise direction (ABCD). Note that the amount of torsion jumps between a^2 and $-a^2$ for every saccade, but that the 3D position of the eye in A is identical at the start and at the end of the trajectory. Therefore, no accumulation of torsion has occurred [20]. Note also that the Donders’ surface for eye positions is strongly twisted in 3D rotation vector space. The torsional component of the Fick Donders’ surface is taken from Eq. (31) and is given by⁵:

$$\mathbf{r}_x = -\tan(\theta_F/2) \cdot \tan(\varphi_F/2) = -\mathbf{r}_y \cdot \mathbf{r}_z \quad (32)$$

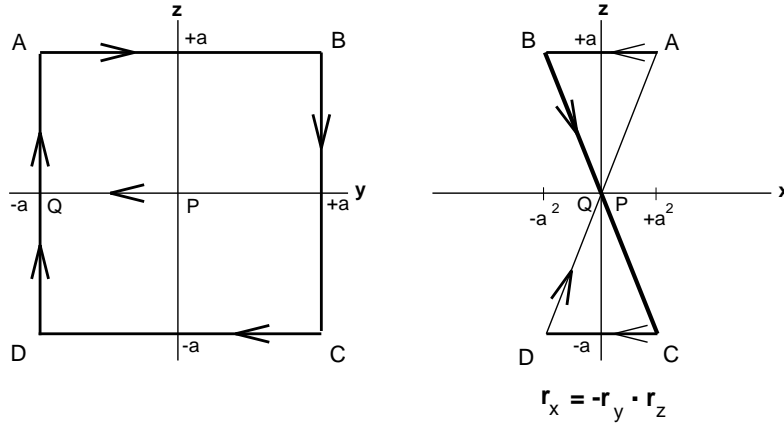


Fig. 7: Donders’ surface produced by a two-axis Fick gimbal system. Note that the resulting surface of gaze positions is markedly twisted in 3D rotation vector space. Thick line (BC) symbolizes positive y -components of gaze position, thin line (DA) negative y -components. As torsion jumps between $\pm a^2$, it does not accumulate during repeated clockwise tracking of the targets.

The nonlinear dependence of \mathbf{r}_x on the gaze coordinates reflects the curved-ness of the Donders’ surface. In addition, the sign of ocular torsion changes,

⁵In the (early) oculomotor literature this gimbal-induced torsion has been termed ‘false torsion’ [3]. To comply with Listing’s law Eq. (33), an additional rotation about the rotated visual axis, $\hat{\mathbf{e}}''_x$, is needed to null this torsion.

each time one of the gaze coordinates changes sign. The proportionality factor of -1 in Eq. (32) is called the *twist score* of the Fick surface [20]. Different types of gimbal system give rise to different twist scores. For example, in the same way one may construct the Donders' surface for a Helmholtz gimbal, by reversing the order of the two rotations Eq. (31) into a horizontal (head-fixed), followed by a vertical (eye-fixed) rotation. In this case, the twist score will be $+1$.

Listing's law. Helmholtz put a specific constraint on the torsional component of eye position, by following a suggestion made earlier by the German physicist Listing [27]. According to this proposal, the oculomotor system reduces the Donders surface of eye positions Eq. (30) to a plane (Listing's plane, LP) when the head is in an upright and stationary position, and the eyes fixate points at optical infinity (no vergence). Therefore, under these experimental conditions, the torsional component of eye position is a linear function of the horizontal and vertical gaze coordinates (Listing's law).

The unique direction perpendicular to LP is defined as the primary position. By a convenient choice of coordinates (which is the primary frame of reference, or the so-called Listing coordinates), all eye positions in Listing's plane have zero torsion (see e.g. Fig. 8 and below) [32,68,77]. Therefore, in the quaternion and rotation vector parametrizations, Listing's law takes a very simple form:

$$\mathbf{r}_x = 0 \quad (33)$$

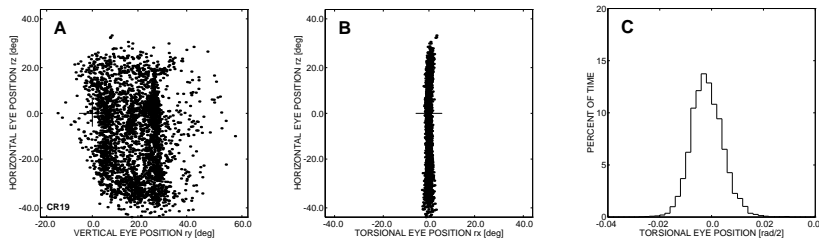


Fig. 8: Listing's law for head-fixed conjugate eye movements of rhesus monkey CR. About 3500 positions of spontaneous eye movements in the light are plotted. Eye positions are plotted as components of rotation vectors (**A**) in the y,z -plane, and (**B**) in the x,z -plane, respectively (scale converted to degrees). Note that Listing's law is well-obeyed. Standard deviation of the width of Listing's plane (**B**) is only 0.6 deg. Panel (**C**) shows a histogram of the torsional components (in half-radians) of eye position for the same data set.

2.5.1 Listing's law for head-fixed saccades.

Thanks to the recent development of accurate recording techniques [5,36], 3D eye movements can be routinely measured with a high spatial and temporal resolution in both man and monkey. Although part of the available data suggests that Listing's law is only approximately valid during fixations [12] and during eye movements [13,54], a majority of studies, performed in several different laboratories, has shown that it is obeyed with remarkable accuracy, both in human [25,43,61] and in monkey [8,33,37,74] subjects (see Fig. 8). The law holds in good approximation for eye fixations, as well as dynamically during saccadic [33,43,61,70] and smooth pursuit [25,63] eye movements (but see also below). It is also equally-well obeyed for saccades toward auditory targets in complete darkness [17], which suggests that Listing's law does not exclusively serve a visual purpose.

Typically, the thickness of Listing's plane (given by the standard deviation of ocular torsion in the primary reference frame, Fig. 8B) is in the order of 0.5-0.7 deg for monkeys [30,70], and about 1.0 deg for human subjects [43]. The plane's thickness is very similar for eye fixations, and for dynamic conditions such as smooth or rapid eye movements along a straight, or along a highly curved trajectory [43].

At this point, it is important to realize that neither Donders' law nor Listing's law simply follow from the infallible laws of physics applied to the plant mechanics since, in principle, there are many different ways in which the oculomotor system could have reduced the number of degrees of freedom for gaze orientations.

For example, eye positions produced by the VOR do *not* obey either Donders' or Listing's law. During torsional vestibular stimulation, $\omega_h = (\dot{\rho}, 0, 0)$, the eye may look into the primary gaze direction ($\mathbf{r}_y = \mathbf{r}_z = 0$) with many different torsional components (violation of Donders' law, Eq. (30)). In the absence of any additional mechanism, ocular torsion would accumulate until it would reach the physical limits of the oculomotor range (see above, Fig. 5). However, the vestibular system prevents such an accumulation by generating torsional 'reset' quick-phases of nystagmus that repeatedly bring the eye back to a position close to zero torsion [6,33].

A second example concerns the binocular viewing of targets in depth. A large body of experimental evidence from different laboratories shows that both eyes violate Listing's law when viewing near targets. The violation, however, follows a clear geometric pattern. Both eyes rotate temporally ('excyclotorsion') when the elevation of the eyes is downward, whereas they rotate nasally ('incyclotorsion') for upward elevations. Listing's law is preserved only when gaze elevation is zero (in the primary reference frame) [44,45]. When plotting these eye positions in 3D space, the pattern resembles that of a Helmholtz two-axis gimbal system (see above), and therefore nicely adheres to Donders' law (a curved surface with a positive twist score close to one, i.e. a full-angle tilt of the angular velocity vector as function

of eye elevation) [44,76].

Yet, as will be argued below, the exact properties of the oculomotor plant do have implications for the way in which the circuitry of the brainstem burst generators and neural integrators is organized, since it should compensate for any (nonlinear) peculiarities in the plant mechanics (see also above, for the 1D case). Regarding the modeling of the 3D saccadic system, however, it is reasonable to suppose that:

- Identical motoneuron firing patterns yield identical eye positions in the head, regardless of plant mechanics and task conditions.
- Ocular torsion may take any value within the oculomotor range (i.e. not restricted by plant mechanics), but it is constrained by the oculomotor task (i.e. the neural commands).

2.5.2 Spontaneous violations of Listing's law

Although Listing's law is well obeyed by the monkey oculomotor system (at least for the head straight up and not moving, and the eyes looking at infinity), the data in Fig. 8C clearly indicate that it is not perfect. Occasionally, small (up to about 2.5 deg) spontaneous excursions from LP are made that are not due to blinks. Such torsional 'errors' are relatively infrequent (in 23% of the saccades, averaged over six monkeys, the displacement exceeds 1.0 deg) but, if present, the torsional component of the eye movement appears to be synchronized with the horizontal and vertical saccade components (see e.g. Fig. 9A). It should be noted, however, that torsional onset is usually better synchronized with the horizontal/vertical components, than torsional offset. Like was observed for the horizontal and vertical components in earlier 2D studies (see above), component stretching seems to be a phenomenon that affects all three saccade components.

Thus, it appears that these torsional displacements are produced by the *saccadic* system. Closer inspection of the eye movement traces indicated that under these circumstances the eye does not drift back passively into the plane, but may stay at the new torsional level for several hundreds of msec (Fig. 9A). We observed that the system typically produces an active 'reset' of ocular torsion by the next saccadic eye movement [31,73,74].

To further quantify this property, we analyzed to what extent the spontaneously occurring violations of Listing's law are corrected by the saccadic system. The results, valid for all monkeys studied so far, show a highly significant relation between the torsional onset position of the eye, \mathbf{r}_x , and the subsequent torsional displacement, \mathbf{d}_x , of the next spontaneous saccade (see Fig. 9B). Multiple linear regression on the data showed that the corrective torsional displacement is solely determined by the torsional onset position, and is neither related to the horizontal/vertical components of eye position, nor to the saccade direction [73].

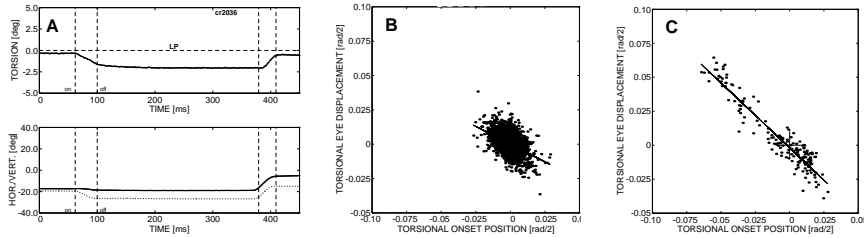


Fig. 9: Spontaneous violations of Listing’s law (**A,B**) by the saccadic system are reset by the next saccade. In panel (**A**) an example of such a violation (with about -2 deg a particularly large one), as well as the subsequent reset saccade are both shown. Panel (**B**) shows, for the entire data set of Fig. 8, that there exists a highly significant relation ($r=-0.49$; $N=3522$) between torsional onset position of the eye (ordinate), and the saccadic torsional displacement of the following saccade (abscissa). Slope of the regression line is $b=-0.52$ (but note that violations and resets are pooled here). An accurate saccadic reset is also generated, when the violation is due to electrical microstimulation in the NRTP (**C**). The range of torsional onset positions is markedly expanded by this experiment (up to 10 deg). Correlation: $r=-0.95$, slope: $b=-0.95$; $N=165$ (i.e. no overshoots; after [73]). These data show that both the saccade burst generator and the neural position integrator of the ocular *saccadic* system are 3D.

The ability of the saccadic system to generate a torsional reset movement has also been shown by electrical microstimulation experiments in the monkey brainstem. Prolonged stimulation of the vertical/torsional burst generator in the riMLF produces a vertical/ipsi-torsional eye movement at constant velocity (torsion may reach levels exceeding 10 deg; [29]). Microstimulation in the precerebellar nucleus reticularis tegmenti pontis (NRTP) yields staircases of horizontal/torsional saccades. Here, the direction of the torsional component depended on the location of the stimulation electrode within the NRTP [74]. Yet, also in these cases, the saccadic system generates a precise torsional reset at the next spontaneous saccade following the stimulation train (see Fig. 9C for an example of the NRTP stimulation results). It is important to realize that the large torsional components in these reset saccades were generated in the absence of any vestibular or optokinetic stimulation and were precisely aimed at Listing’s plane.

These results therefore clearly indicate that both the saccadic burst generator as well as the eye position neural integrator carry a 3D eye-movement code, and that Listing’s law is actively controlled by neural commands. As will be discussed below, however, the type of 3D signal used by these structures (i.e. coordinate velocity $\dot{\mathbf{r}}$ vs. angular velocity, ω) cannot be decided on the basis of these experiments.

Interestingly, a localized reversible inactivation of the NRTP appeared to interfere with the capacity of the saccadic system to reset the torsional component into LP [74].

2.5.3 Parametrization of 3D saccades.

From Listing's law Eq. (33) it follows, that when the eye makes a movement from one Listing position, \mathbf{r}_1 , to a new Listing position, \mathbf{r}_2 , it can do so by spinning about the unique single-axis of rotation that is given by the quotient vector:

$$\mathbf{q} = \mathbf{r}_2 \circ \mathbf{r}_1^{-1} \quad \text{because} \quad \mathbf{q} \circ \mathbf{r}_1 = \mathbf{r}_2 \quad (34)$$

Applying the product rule for rotation vectors Eq. (27):

$$\mathbf{q} = \frac{\mathbf{r}_2 - \mathbf{r}_1 + \mathbf{r}_1 \times \mathbf{r}_2}{1 + \mathbf{r}_1 \bullet \mathbf{r}_2} \approx \mathbf{d} + \mathbf{r}_1 \times \mathbf{d} \quad (35)$$

where the approximation holds up to $\mathcal{O}(\rho^3)$, and we have introduced the *difference vector* in LP:

$$\mathbf{d} \equiv \mathbf{r}_2 - \mathbf{r}_1 \quad (36)$$

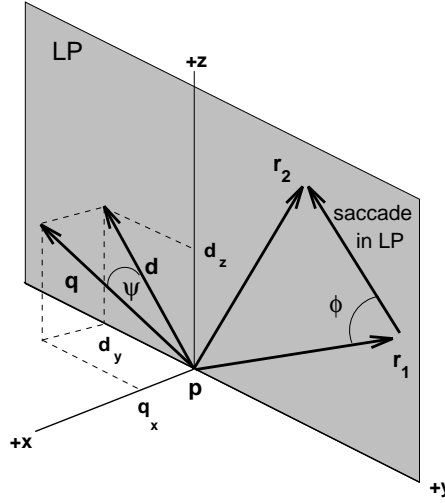


Fig. 10: Eye positions in Listing's plane (LP, shaded) at the onset (\mathbf{r}_1) and offset (\mathbf{r}_2) of a head-fixed saccade. The difference vector, (\mathbf{d}) lies in LP, but the quotient vector, (\mathbf{q}) is tilted out of the plane by angle ψ . \mathbf{p} : primary position.

Note that the quotient vector \mathbf{q} is parallel to the angular velocity vector (cf. with Eq. (28) and use the fact that $\mathbf{d} \parallel \dot{\mathbf{r}}$). Thus, despite the fact that the initial and final eye positions belong to LP, the actual ocular rotation axis 'tilts' out of LP (i.e. $\mathbf{q}_x \neq 0$) by an amount that depends on the displacement amplitude, the initial eye position eccentricity, and the angle, ϕ , between \mathbf{r}_1 and \mathbf{d} :

$$\mathbf{q}_x = \mathbf{r}_{1,y} \cdot \mathbf{d}_z - \mathbf{r}_{1,z} \cdot \mathbf{d}_y = |\mathbf{d}| \cdot |\mathbf{r}_1| \sin(\phi) = |\mathbf{d}| \cdot \mathbf{r}_1^\perp \quad (37)$$

Although \mathbf{q} can attain almost any angle with LP, this property has become known in the oculomotor literature as the '*half-angle rule*' (e.g. [15]; see Appendix A-3, for more details). The geometric relation between the quotient and difference vectors and LP is further illustrated in Fig. 10.

A saccadic eye movement between two positions in LP can now be parametrized in two different ways [33,70]. The first description considers a saccade as the unique *single-axis rotation* that brings the eye from initial position \mathbf{r}_1 into final position \mathbf{r}_2 , through the quotient vector Eq. (35). This vector is related to angular velocity by:

$$\mathbf{q} = \int_{t_1}^{t_2} \boldsymbol{\omega}(t) dt \quad (38)$$

Note, that Eq. (34) may be interpreted as a straightforward 3D extension of the concept of *eye motor error*. However, this vector depends not only on the difference between the initial and final eye positions (as in 1D and 2D saccade descriptions), but also on the absolute initial eye position (unlike the 1D and 2D case). Note also that in this parametrization the saccade vector has *three* degrees of freedom Eq. (37), by following the half-angle rule, although the eye positions are constrained to a plane (Fig. 10).

Alternatively, a saccade may also be characterized as the *difference* vector between the two Listing positions Eq. (36), which is related to the coordinate velocity by:

$$\mathbf{d} = \int_{t_1}^{t_2} \dot{\mathbf{r}}(t) dt \quad (39)$$

Since the difference vector is constrained to LP (at least for eye movements in LP), it has only *two* degrees of freedom.

A nontrivial property of the rotation vector description is, that the trajectory of the eye for a single-axis rotation between two Listing positions, say \mathbf{r}_1 and \mathbf{r}_2 , follows a straight line in LP. That is, for all times between saccade onset and saccade offset, the trajectory of the eye is determined by⁶:

$$\mathbf{r}(t) = \mathbf{r}_1 + \sigma(t) \cdot (\mathbf{r}_2 - \mathbf{r}_1) \quad (40)$$

where $\sigma(t)$ is the normalized saccade amplitude [30].

⁶To show that the trajectory of a single-axis rotation in Listing's plane is a straight line one considers the rotation Eq. (35) as a function of time (i.e. the axis is fixed in space, but the rotation amplitude, $\tan(\rho_{12}/2) = \tan(\rho_{12}(t)/2) \equiv \sigma(t) \tan(\rho_{12}/2)$, with $\sigma(t)$ strictly increasing between 0 and 1). The movement from Listing position \mathbf{r}_1 to \mathbf{r}_2 is then given by the time-dependent quotient vector Eq. (34), $\mathbf{q}(t)$, applied to \mathbf{r}_1 :

$$\mathbf{r}(t) = \mathbf{q}(t) \circ \mathbf{r}_1 \quad \text{with} \quad \mathbf{q}(t) = \sigma(t)(\mathbf{r}_2 \circ \mathbf{r}_1^{-1})$$

Substitution, and including only terms up to $\mathcal{O}(\rho^3)$, yields:

$$\mathbf{r}(t) \approx \sigma(t)\mathbf{q} + \mathbf{r}_1 + \sigma(t)\mathbf{q} \times \mathbf{r}_1$$

from which all cross-product terms vanish, and Eq. (40) immediately follows. This result is also exact if the higher orders in rotation angle ρ are included [30].

Such a simple geometric property of rotation vectors (i.e. saccades as geodesics in 3D space) could be advantageous for representing the spatial trajectory in the neural programming stage (e.g. in neural motor maps, such as the SC). As mentioned earlier, a fixed-axis rotation in quaternion space is represented by a great-circle arc on the unit sphere, which is not the shortest path between two points.

A further interesting and nontrivial interpretation of the difference vector Eq. (36) is derived from its close correspondence to the *retinal error*, \mathbf{s}_o , of a peripheral visual target (situated at Listing position \mathbf{r}_2), when the fovea is in the initial position, \mathbf{r}_1 . As is further detailed in Appendix A-4 [30,33], the horizontal and vertical coordinates of a visual target relative to the fovea are, in good approximation, linearly related to the components of the desired eye-displacement vector, \mathbf{d} , and therefore *independent* of initial eye position:

$$\begin{aligned} \mathbf{s}_{o,y} &\approx 2 \cdot \mathbf{d}_z \\ \mathbf{s}_{o,z} &\approx -2 \cdot \mathbf{d}_y \end{aligned} \quad (41)$$

where the approximation holds up to $\mathcal{O}(\rho^3)$ for the initial and final eye-position angles (relative to primary position). This approximation is very good in the peri-primary oculomotor range (up to 15 deg), but is still better than 12% for fixations up to 30 deg away from primary position (which is about the range of normal saccade accuracy).

2.5.4 3D Models: the Saccade Programmer.

The two different parametrizations, \mathbf{d} vs. \mathbf{q} , suggest quite different possibilities for the neural organization of the saccadic system [10,30,33,52,60,62,70]. In principle, either description could represent the neural signal that is encoded by the saccade programmer as the desired position or displacement of the gaze line.

In Fig. 11A a visual double-step paradigm is illustrated for two different trials, in which the saccadic system has to program two different sequences of saccades to foveate the two targets: AB followed by BC, vs. AB' followed by B'C.

In the simplest 3D model (the so-called *Vector model* [30], further detailed below), the programming stage of the saccadic system only involves *commutative*, vectorial computations, in which the coordinates of the next saccade vector are updated according to the approximation scheme suggested by Eq. (41).

With the eye initially in Listing position A, the two targets of the double-step jump, B (or B') and C, define the retinal error vectors \mathbf{s}_{AB} (or $\mathbf{s}_{AB'}$), and \mathbf{s}_{AC} , respectively.

Since both retinal error vectors correspond closely (up to $\mathcal{O}(\rho^3)$) to the respective eye-displacement vectors \mathbf{d}_{AB} ($\mathbf{d}_{AB'}$) and \mathbf{d}_{AC} in LP Eq. (41), the Vector model takes these approximative, but linear, estimates as the desired

saccade program. For the different sequences, the two saccades are therefore computed as:

$$\mathbf{d}_{AB^{(t)}} = \mathbf{s}_{AB^{(t)}} \quad \text{and} \quad \mathbf{d}_{B^{(t)}C} = \mathbf{s}_{AC} - \mathbf{d}_{AB^{(t)}} \quad (42)$$

Note, that in this model the sequences A-B-C vs. A-B'-C involve the programming of two *identical* sets of saccade displacement vectors, that are to be executed in reversed order (commutative program, see Fig. 11B).

From an experimental point of view, this model therefore predicts that cell activity at sites encoding desired saccade displacement vectors in the double-step paradigm (as has been hypothesized e.g. for the cortical frontal eye fields (FEF), the posterior parietal cortex (PPC), and the midbrain SC) will show *no* difference for saccades into their movement field, regardless the order in which they are elicited.

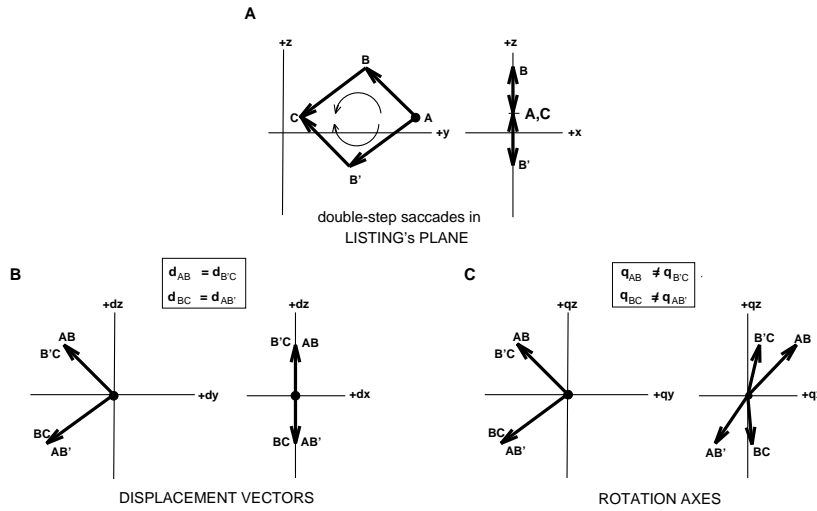


Fig. 11: Illustration of the differences between the programming stages of the Vector and Quaternion models for two different double-step trials that move the eye between initial position A to final position C in LP (**A**) (see also Fig. 12). The Vector model has a commutative saccade programmer, according to Eq. (41). Since the resulting displacement vectors are independent of initial eye position, saccades in the double-step trials are identical (**B**). The Quaternion model (**C**) has a noncommutative programmer that computes the required rotation axis coordinates through Eq. (35). This results in different saccade codes for the different sequences.

In the mathematically exact *Quaternion model* (see below), the saccades are programmed as desired *rotations* from initial to final eye position Eq. (35). Therefore, the retinal error vectors need to be transformed into the appro-

priate quotient vectors according to:

$$\begin{aligned} \text{A-B-C sequence: } \quad \mathbf{q}_{AB} &= \mathbf{r}_B \circ \mathbf{r}_A^{-1} & \text{and} & \quad \mathbf{q}_{BC} = \mathbf{r}_C \circ \mathbf{r}_B^{-1} \\ \text{A-B'-C sequence: } \quad \mathbf{q}_{AB'} &= \mathbf{r}_{B'} \circ \mathbf{r}_A^{-1} & \text{and} & \quad \mathbf{q}_{B'C} = \mathbf{r}_C \circ \mathbf{r}_{B'}^{-1} \end{aligned} \quad (43)$$

In this model, the saccade codes of the programmer do differ when the sequence is reversed, because the rotation axis depends on the initial eye position (noncommutative quaternion multiplication, where \mathbf{q}_x is of second order in the saccade amplitude, $\mathcal{O}(\rho^2)$; see Fig. 11C). Cell activity in a quaternion programmer is therefore expected to yield different firing patterns for the two double-step configurations. Moreover, electrical microstimulation at such a site (encoding the desired eye rotation \mathbf{q}_{site}) should lead to an eye-position dependent violation of Listing's law, since the stimulation would bypass the noncommutative programming stage [70]:

$$\mathbf{r}_{\text{stim}} = \mathbf{q}_{\text{site}} \circ \mathbf{r}_o \quad \text{from which: } \quad \mathbf{r}_{\text{stim}}^x = |\mathbf{q}_{\text{site}}| \cdot |\mathbf{r}_o| \cdot \sin(\phi) \quad (44)$$

with ϕ the angle between \mathbf{q}_{site} and initial eye position \mathbf{r}_o . Recent experimental data from the monkey SC have not provided support for the quaternion programming scheme, since both microstimulation and complete reversible collicular inactivation still resulted in saccades that obeyed Listing's law ($\mathbf{r}_{\text{stim}}^x = 0$) [70]. Moreover, movement fields appeared to be better described in terms of desired eye displacements in LP, \mathbf{d} , rather than in desired eye rotations, \mathbf{q} [33,70].

Still, conclusive evidence is lacking to either refute or prove either model of the saccade programmer for the following reasons: One complicating factor is the recent result that the movement fields of cells in the SC *do* seem to possess an eye-position related component [72]. However, changes in eye-position do not affect the optimal direction of the cell's movement field (i.e. the center of the movement field is unrelated to eye position) but, instead, seem to have a modulatory (multiplicative) influence on the cell's firing rate. A subsequent theoretical study showed that with a population of such so-called 'gain-field' cells, the SC could provide an accurate estimate of the 3D desired rotation axis of the eye, despite the fact that the individual cells are tuned to relative eye displacements only [69].

Furthermore, the exact site of the saccade programming stage is still a matter of debate. So far, most studies assume that the deep layers of the SC issue a desired motor command to the burst generator. More recent experiments indicate, however, that the signal sent by the SC can still be modified substantially by downstream premotor structures without the SC being 'aware' of these changes. For example, Stanford and Sparks provided evidence that SC movement fields are better described in *visual* coordinates than in *motor* coordinates, because the systematic mislocalizations of saccades to remembered visual targets are not reflected in a cell's activity [53]. A similar conclusion was drawn by Frens and Van Opstal on the basis of short-term saccadic gain adaptation experiments. In this paradigm,

a consistent intrasaccadic target displacement causes the gain of saccade amplitudes to decrease accordingly. Yet, the cell's movement-related activity does not change, but stays better tuned to the original (not displaced) retinal-error vector [18].

These experiments suggest that the SC may actually send an (updated) *retinal error* signal to the brainstem, rather than a desired eye *motor* command. At the next level, this signal could be combined with signals about absolute eye- and head position and get transformed into the appropriate frame of reference for the control of orienting eye-, head-, and body movements. Such a suggestion has recently been made by Goossens and Van Opstal [22] in order to explain the eye-head gaze-shift patterns of human subjects to auditory and visual targets (see above, Fig. 3), as well as by Tweed [58] on theoretical grounds (see below, Fig. 13).

2.5.5 3D Models: the Saccade Generator.

The burst generator. In the subsequent stage of the saccadic system, the burst generator transforms a (current) motor error signal (constructed by internal feedback) into an eye velocity (and acceleration) signal (the pulse; see also above, Fig. 1B,C). The process of pulse-step generation also necessitates the integration of the eye-velocity pulse into a neural estimate of absolute eye position. Because the integral of eye angular velocity does not yield eye position (e.g. Fig. 5), an important question is whether the burst generator issues either a coordinate velocity, $\dot{\mathbf{r}}$, or an angular velocity signal, ω .

In the two extreme versions of possible 3D saccade models presented here, the Vector model (Fig. 12A) proposes that the burst generator provides a coordinate velocity output. In contrast, the Quaternion model (Fig. 12B) assumes the generation of an angular velocity signal. There are several important consequences attached to these two conceptually different neural codes [30,60]:

- Because the 'half-angle rule' requires the rotation axis to tilt with respect to LP as function of eye position (Eqn. 35), the activity of cells in the quaternion burst generator should depend on absolute eye position (i.e. the number of spikes in the burst is proportional to $|\mathbf{q}|$, Eqn. 38). By contrast the vectorial burst generator should be insensitive to changes in initial eye position (Eqn. 39).
- The input to the neural position integrator should be proportional to coordinate velocity (but may contain coordinate acceleration signals as well). In the Quaternion model, an eye-position dependent, non-commutative transformation is needed to convert angular velocity into coordinate velocity (Eqn. 29). Note that the weeding out of angular acceleration signals is less trivial (Eqn. 24).

- In the eye-displacement scheme (Fig. 1C), feedback of velocity should be transformed into current eye displacement, $\mathbf{d}(t)$. According to the Quaternion model, this displacement is constructed by an eye-position dependent resettable integrator. The output of the burst generator in the Vector model may be linearly integrated to provide eye displacement.
- In the implementation of feedback, a desired movement signal is compared to some internal neural estimate of the actual movement. In the Vector model, these comparisons are achieved by commutative vectorial subtractions. For example, the input to the vectorial burst generator is a current motor error signal that is computed as a difference vector: $\mathbf{d}^*(t) = \mathbf{d}_L - \mathbf{d}(t)$. In the Quaternion model, however, the desired rotation is compared to the current movement by rotation vector *division* (Eqn. 35): $\mathbf{q}(t) = \mathbf{q}_d \circ \mathbf{d}^{-1}(t)$.

In the discussion of the 1D (and 2D) saccadic system, it became clear that the entire pulse-step generating circuit is needed to counteract the sluggishness (viscosity and elasticity) of the oculomotor plant. Therefore, the dynamics of the 3D oculomotor plant play an important role in the organization of the neural circuitry that is designed to control it, and may explain the need for either coordinate or angular velocity inputs as its drive.

3D oculomotor plant. To extend the 1D plant model to three dimensions, the motoneuron signal has to be treated as a three-dimensional vector, $\mathbf{t}(t)$, which now represents the direction of the net torque acting on the plant. For example, if only the left lateral rectus muscle (LLR) is innervated, with the eye in the primary position, its action can be described by a torque acting in the positive vertical direction, i.e. $\mathbf{t}_{LLR}(t) \propto \text{MN}(t) \cdot \hat{\mathbf{e}}_z$. As a result, the eye will rotate about the vertical axis, so that its angular velocity vector will be aligned with \mathbf{t} . The total torque acting on the plant is the vectorial sum of the individual muscle torques, and when the eye attains a fixed position, the net torque should be zero (because the eye does not translate, the sum of the forces on the globe is always zero). There is some controversy to what extent the direction of each muscle's torque vector depends on eye position, i.e. whether

$$\mathbf{t}_i \stackrel{?}{=} \mathbf{t}(\mathbf{r})_i \quad i = 1 \dots 6 \quad (45)$$

This is not a trivial problem, since the total torque depends on the different forces acting on the globe. For every muscle, $\mathbf{t}_i = \mathbf{c}_i \times \mathbf{F}_i$, where \mathbf{c}_i is the position vector of the muscle pointing from the center of the eye to the point where it leaves the globe. This effective point of insertion may shift for different eye positions, thus changing the direction of that muscle's torque vector. The forces in turn are determined by each muscle's individual (eye-position dependent) and nonlinear length-tension and force-velocity relations (muscles behave as nonlinear springs, although part of the

in order to formulate an adequate model of the 3D plant. Moreover, the elasticity and viscosity parameters of the plant are now described by 3×3 (possibly anisotropic) matrices, instead of by single scalars.

The following two, highly simplified 3D plant models capture the essentials of the problem, because each gives rise to a very different 3D saccade model (Fig. 12).

In the so-called *linear plant model* [30,64], it is assumed that the muscle torques *do* depend on eye position, but in such a way that when the net innervation of the motoneurons, $\mathbf{t}(t)$, is confined to Listing's plane, the eye will precisely follow the half-angle rule and move along a trajectory in Listing's plane. In this model, the burst signal, $\mathbf{b}(t)$ should be independent of eye position, and is taken to be proportional to the coordinate velocity vector, $\dot{\mathbf{r}}$. The neural integrator, \mathbf{n} may linearly integrate the phasic burst signal (note that contributions of eye acceleration in this signal will not survive the integration, see Eq. (1)). The linear plant model is therefore determined by the following dynamical system, which is a straightforward extension of the 1D Robinson model given in Eq. (3) [30,64]:

$$\begin{aligned}\dot{\mathbf{n}} &= \mathbf{b} \\ \mathbf{t} &= [C]\mathbf{n} + [D]\mathbf{b} \\ \dot{\mathbf{r}} &= [V]^{-1}(\mathbf{t} - [K]\mathbf{r})\end{aligned}\tag{46}$$

Here, $[C]$ and $[D]$ are the 3×3 brainstem connection matrices to the three antagonist muscle pairs that embody a neural model of the plant, whereas $[K]$ and $[V]$ are the actual plant elasticity and viscosity tensors. Again, adequate pulse-step matching requires that $[C] = [K]$ and $[D] = [V]$ (in more realistic models, these matrices could incorporate eye position- and velocity-related nonlinearities, but since the brainstem - cerebellar circuitry may cope with any complexity of the actual plant, this doesn't change the basic argument).

By contrast, in the *nonlinear plant model* [60,64], the muscle torques do *not* depend on eye position, so that the directions remain fixed in the head. As a consequence, the net innervation to the plant needs to account for the eye position-dependent tilt of the angular velocity vector (i.e. the burst generator should encode $\omega(t)$), and the input to the neural integrator, $\dot{\mathbf{n}}$, now depends nonlinearly on eye-position. This leads to the following set of model equations (where the noncommutative multiplication rule Eq. (29) for rotation vectors has been applied):

$$\begin{aligned}\dot{\mathbf{n}} &= \mathbf{b} + \mathbf{b} \times \mathbf{n} + (\mathbf{b} \cdot \mathbf{n})\mathbf{n} \\ \mathbf{t} &= [C]\mathbf{n} + [D]\mathbf{b} \\ \omega &= [V]^{-1}(\mathbf{t} - [K]\mathbf{r})\end{aligned}\tag{47}$$

Alternatively, pulling directions of eye muscles could even be assumed to be eye-fixed (i.e. the net-torque on the globe follows a 'full-angle' rule), although this possibility seems unrealistic considering the current anatomical

evidence [11]. Presumably, more realistic models of the plant will lie somewhere between the perfect half-angle and zero-angle extremes of Eq. (46) and Eq. (47).

2.6 Head-free saccadic gaze shifts in 3D.

When the head is also free to move in 3D, the problem gets considerably more complicated. In this section we will not go into too much detail, but restrict the description to the essential new points that arise. First, it should be noted, that in this case the relevant variables are the head position and velocity in space, the eye position and velocity in space (or gaze), and the eye position and velocity in the head. Since the eye is moved by the head in the spatial frame of reference, the kinematics of gaze are described as the result of an active rotation of the head in space, followed by the *passive* rotation of the eye in the rotated head, i.e.

$$\mathbf{g} = \mathbf{e}' \circ \mathbf{h} = \mathbf{h} \circ \mathbf{e} \quad (48)$$

where in the right-hand part of Eq. (48) both vectors are expressed in spatial coordinates. The eye position in the head is therefore given by

$$\mathbf{e} = \mathbf{h}^{-1} \circ \mathbf{g} = \frac{\mathbf{g} - \mathbf{h} + \mathbf{g} \times \mathbf{h}}{1 + \mathbf{g} \bullet \mathbf{h}} \quad (49)$$

and the ocular torsion in the head is therefore

$$\mathbf{e}_x \approx \mathbf{g}_x - \mathbf{h}_x + \mathbf{g}_y \cdot \mathbf{h}_z - \mathbf{g}_z \cdot \mathbf{h}_y \quad (50)$$

Note that if gaze and head positions would adhere to Listing's law, the eye in the head in general will not. There are several complicating factors in the analysis and modeling of 3D head-free gaze shifts. First, the eye and the head may move at different speeds, in different directions, and usually do not start simultaneously [20,22,58,65]. Second, the eye reaches the target well before the end of the (slower) head movement, which invokes the re-activation of the VOR. The vestibular system encodes head-angular velocity in 3D and is not concerned with Listing's law, or even Donders' law (see above). So how is the synergy between the oculomotor, the head motor and the vestibular systems organized?

Recent experiments in which large head-free gaze shifts were recorded have revealed the following principles [20,65]:

- The head follows Donders' law, rather than Listing's law. Head position data can be reasonably well described by a surface produced by a two-axis Fick gimbal (with a twist score of about -0.5, see above).
- For oblique gaze shifts, the head moves predominantly in the horizontal direction, and much less in the vertical direction (i.e. against gravity). The reverse is true for the eye in the head. Because of this, gaze positions in space are also confined to a Fick-like Donders' surface resembling that of the head.

- *During* the gaze shift, the eye in space is *neither* constrained by Listing's law, nor by Donders' law. Instead, the gaze trajectories curve away from the Donders' surface determined by the static gaze positions. This finding can be understood when it is realized that the eye is driven toward a *saturated* position of the eye in space. The 3D saturation prevents the eye from running into the borders of the oculomotor range (OMR; see also Fig. 3).
- *After* the gaze shift is over (i.e. eye is on target and the head at rest), gaze-in-space position again follows Donders' law, and eye position in the head is approximately constrained by Listing's law. The latter finding is approximate in the sense that LP is not exactly fixed in the head but shifts with head orientation re. gravity. Most notably, for head-roll positions, a static torsional counterroll of eye-in-head results that may reach about 5 deg.

In a recent 3D extension of current eye-head control models (such as discussed above, and shown in Fig. 3), Tweed [58] introduced several additional features that lead to a successful reproduction of measured eye-head trajectories. A schematic outline of this model is presented in Fig. 13. One important feature is that eye and head are controlled by their own oculocentric (\mathbf{e}_d) and craniocentric (\mathbf{h}^*) motor signals, respectively, driven in independent local feedback modes. The head motor system incorporates the experimental findings that the desired end position complies with Donders' law, and that the horizontal and vertical motor error components are different.

A second novel property of the model concerns a proposal for the signal that drives the oculomotor system. In the model, the eye is controlled by a desired position in space (\mathbf{g}^*), but in such a way that at the *end* of the gaze shift eye position in the head (\mathbf{e}^*) will obey Listing's law. Note that this proposal includes a *neural* Listing's law operator interposed between the 2D representation of the SC output (which presumably encodes the updated initial gaze error signal, $\Delta\mathbf{g}_d$) and the oculomotor burst generator. Note also, that the desired eye position itself is *not* constrained by Listing's law (it may have a considerable torsional component), because it has to take the additional (Donders) head movement (and concomitant 3D VOR response) into account that may still proceed after the eye has acquired the target.

The noncommutative computations embedded in the Listing operator incorporate both the position of the target in space (which is transformed from the 2D retinal error input, $\Delta\mathbf{g}_d$, into a spatial code, \mathbf{g}_d), and the desired position of the head as constrained by Donders' law (\mathbf{h}^*). However, the desired eye position in space cannot be used directly by the oculomotor system, since the eccentricity of this signal often far exceeds the OMR. Therefore, before the signal is passed to the oculomotor burst generator, it is updated as a 3D clipped craniocentric eye position signal ($\mathbf{e}_d^{\text{sat}}$) that ensures that the eye motor error command incorporates the current head

movement, and does not run into the physical limits imposed by the OMR (for specific details, see [58]).

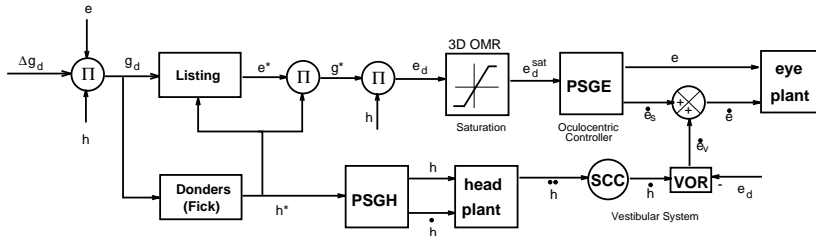


Fig. 13: Three-dimensional proposal of eye-head control model by Tweed [58]. The model is driven by a desired eye position in space (gaze, g_d), which is transformed by the Listing operator into a desired eye position in the head (e^*), such that the eye will obey Listing's law at the *end* of the eye- and head movement. Note, that due to the interaction with the VOR (at the moment of target acquisition), this signal should have three degrees of freedom (is *not* in LP!). The desired gaze shift is transformed by the Donders' operator (modeled by a Fick-like gimbal) into a desired head-in-space signal, h^* , that drives the pulse-step generator of the head motor system. This signal is also transformed into desired gaze-in-space for the eye (g^*). The oculomotor burst generator is driven by eye motor error (like in Robinson's model of Fig. 1), where the desired eye position in the head is clipped by a 3D saturation. The eye- and head plants are assumed to be linear. Π : noncommutative quaternion products. Local feedback loops are omitted for clarity. Compare also with Fig. 3. After [58].

Both the oculomotor and head pulse-step generators are matched to linear plant models, which ensures that the neural position integrators can operate in a linear mode, and that both burst generators issue coordinate velocity and acceleration signals (see also above). Like in the model of Fig. 3, the VOR is inactivated by the current eye motor-error signal (e_d).

2.7 Conclusion.

In conclusion, the noncommutative kinematic principles of 3D rotations that underlie the control of orienting gaze shifts are most likely embedded to a large extent in the central nervous system, and are not due to mechanical interactions at the level of the motor plant. Although linear mechanical models of the plant may in principle account for the 'half-angle rule'-behavior of ocular saccades in Listing's plane (note that the behavior of the muscle torques under dynamic conditions is unknown), they are unable to account for a myriad of other 3D kinematic aspects of gaze control:

- The existence of an active (saccadic) error correction mechanism that ensures that the eye stays very close to LP (within 0.6 deg) despite substantial occasional errors. This mechanism prevents torsional accumulation (due to a random walk), and shows that the saccadic burst generator and eye position integrator represent eye movements in 3D, rather than in 2D retinal coordinates.
- The deficit in torsional error correction after local inactivation of the NRTP.
- The different movement strategies used by the eye and head control systems under head-fixed (Listing) and head-free (Donders) conditions.
- The necessity for a transformation of head (angular) velocity signals of the VOR into appropriate eye (coordinate) velocity signals that can be readily integrated by a position and displacement neural integrator.
- The Helmholtz-gimbal behavior of the binocular disjunctive vergence system (full-angle elevation-dependence of ocular torsion).
- The systematic dependence of the orientation of LP on head position relative to gravity.
- The systematic shift of LP after unilateral inactivation of neurons in the vertical/torsional burst generator of the riMLF.

Acknowledgements:

Supported by the University of Nijmegen, The Netherlands. This paper leans heavily on the outstanding work of many colleagues, most notably, Klaus Hepp, Tutis Vilis, Douglas Crawford and Douglas Tweed. I dedicate this paper to the memory of our unforgettable assistant Vappu Furrer-Isoviita, and our dear colleague Volker Henn.

Selected references

- [1] **Bizzi, E., Kalil, R.E., and Tagliasco, V.** (1971) Eye-head coordination in monkeys: evidence for centrally patterned organization. *Science* **173**: 452-454
- [2] **Brand, L.** (1948) *Vector and tensor analysis*, pp. 403-429. Wiley, New York, USA.
- [3] **Carpenter, R.H.S.** (1988) *Movements of the eyes*, pp. 156-165, Pion, London
- [4] **Cannon, S.C. and Robinson, D.A.** (1987) Loss of the neural integrator of the oculomotor system from brain stem lesions in monkey. *J. Neurophysiol.* **57**: 1383-1409
- [5] **Collewijn, H., Van der Mark, F. and Jansen, T.C.** (1987) Precise recording of human eye movements. *Vision Res.* **15**: 447-450
- [6] **Crawford, J.D.** (1994) The oculomotor neural integrator uses a behavior-related coordinate system. *J. Neurosci.* **14**: 6911-6923

- [7] **Crawford, J.D.** (1997) Geometric transformations in the visual-motor interface for saccades. In: *Three-dimensional kinematics of eye-, head-, and limb movements*, (Fetter, M., Tweed, D. and Misslisch, H., eds), Harwood Academic Publ., Amsterdam, pp. 85-99.
- [8] **Crawford, J.D. and Vilis, T.** (1992) Symmetry of oculomotor burst neuron coordinates about Listing's plane. *J. Neurophysiol.* **68**: 432-448
- [9] **Crawford, J.D., Cadera, W. and Vilis, T.** (1991) Generation of torsional and vertical eye position signals by the interstitial nucleus of Cajal. *Science* **252**: 1551-1553
- [10] **Crawford, J.D., and Guitton, D.** (1997) Visual-motor transformations required for accurate and kinematically correct saccades. *J. Neurophysiol.* **78**: 1447-1467
- [11] **Demer, J.L., Miller, J.M., Poukens, V., Vinters, H.V. and Glasgow, B.J.** (1995) Evidence for fibromuscular pulleys of the recti extraocular muscles. *Invest. Ophthalmol. Vis. Sci.* **36**: 1125-1136
- [12] **Ferman, L., Collewijn, H. and Van den Berg, A.V.** (1987) A direct test of Listing's law. I. Human ocular torsion measured under static conditions. *Vision Res.* **27**: 929-938
- [13] **Ferman, L., Collewijn, H. and Van den Berg, A.V.** (1987) A direct test of Listing's law. II. Human ocular torsion measured under dynamic conditions. *Vision Res.* **27**: 939-951
- [14] **Ferman, L., Collewijn, H., Jansen, T.C. and Van den Berg, A.V.** (1987) Human gaze stability in the horizontal, vertical, and torsional direction during voluntary head movements, evaluated with a three-dimensional scleral induction coil technique. *Vision Res.* **27**: 811-828
- [15] **Fetter, M., Haslwanter, T., Misslisch, H., and Tweed, D.** (eds.) (1997) *Three-dimensional kinematics of eye, head, and limb movements*. Harwood Academic Publishers, Amsterdam.
- [16] **Freedman, E.G., Stanford, T.R., and Sparks, D.L.** (1996) Combined eye-head gaze shifts produced by electrical stimulation of the superior colliculus in rhesus monkeys. *J. Neurophysiol.* **76**: 927-952
- [17] **Frens, M.A. and Van Opstal, A.J.** (1995) A quantitative study of auditory-evoked saccadic eye movements in two dimensions. *Exp. Brain Res.* **107**: 103-117
- [18] **Frens, M.A. and Van Opstal, A.J.** (1997) Monkey superior colliculus activity during short-term saccadic adaptation. *Brain Res. Bull.* **43**: 473-483
- [19] **Galiana, and H.L., Guitton, D.** (1992) Central organization and modeling of eye-head coordination during orienting gaze shifts. *Ann. Acad. Sci.* **656**: 452-471
- [20] **Glenn, B., and Vilis, T.** (1992) Violations of Listing's law following large eye and head gaze shifts. *J. Neurophysiol.* **68**: 309-318.
- [21] **Goldstein, H.** (1980) *Classical Mechanics*. Addison-Wesley, Reading, MA
- [22] **Goossens, H.H.L.M., and Van Opstal, A.J.** (1997) Human eye-head coordination in two dimensions under different sensorimotor conditions. *Exp. Brain Res.* **114**: 542-560

- [23] **Guietton, D., and Volle, M.** (1987) Gaze control in humans: eye-head coordination during orienting movements to targets within and beyond the oculomotor range. *J. Neurophysiol.* **58**: 427-459
- [24] **Hallet, P.E., and Lightstone, A.D.** (1976) Saccadic eye movements toward stimuli triggered by prior saccades. *Vision Res.* **66**: 88-106
- [25] **Haslwanter, T., Straumann, D., Hepp, K., Hess, B.J.M. and Henn, V.** (1991) Smooth pursuit eye movements obey Listing's law in the monkey. *Exp. Brain Res.* **87**: 470-472
- [26] **Haustein, W.** (1989) Considerations on Listing's law and the primary position by means of a matrix description of eye position control. *Biol. Cybern.* **60**: 411-420
- [27] **von Helmholtz, H.** (1867) *Handbuch der physiologischen Optik*, Voss, Hamburg (English translation 1962, Dover, New York)
- [28] **Henn, V., Lang, W., Hepp, K., and Reisine, H.** (1984) Experimental gaze palsies in monkeys and their relation to human pathology. *Brain* **107**: 619-636
- [29] **Henn, V., Straumann, D., Hess, B.J.M., Van Opstal, A.J. and Hepp, K.** (1992) The generation of torsional and vertical rapid eye movements in the riMLF. In: *Vestibular and brainstem control of eye, head, and body movements*, (Shimazu, H. and Shinoda, Y., eds), pp. 177-182, Japanese Scientific Societies Press, Tokyo/S. Karger, Basel
- [30] **Hepp, K.** (1990) On Listing's law. *Commun. Math. Phys.* **132**: 285-292
- [31] **Hepp, K.** (1995) Saccades and Listing's law. in *Handbook of Brain Theory and Neural Networks*, (Arbib, M., ed), pp. 826-830, MIT Press, Cambridge, MA
- [32] **Hepp, K., Henn, V., Vilis, T. and Cohen, B.** (1989) Brainstem regions related to saccade generation. In: *The neurobiology of saccadic eye movements*. (Vol. 3), (Wurtz, R.H. and Goldberg, M.E., eds), pp. 105-212, Elsevier, Amsterdam
- [33] **Hepp, K., Van Opstal, A.J., Straumann, D., Hess, B.J.M. and Henn, V.** (1993). Monkey superior colliculus represents rapid eye movements in a two-dimensional motor map. *J. Neurophysiol.* **69**: 965-979
- [34] **Hepp, K., Suzuki, Y., Straumann, D., Hess, B.J.M.** (1994) On the three-dimensional rapid eye movement generator in the monkey. In: *Information processing underlying gaze control*, (Delgado-García, J.-M., Godeaux, E., Vidal, P.P., eds), pp. 65-74, Pergamon, Oxford
- [35] **Hepp, K., Van Opstal, A.J., Suzuki, Y., Straumann, D., Hess, B.J.M., and Henn, V.** (1997) Listing's law: visual, motor, or visuomotor? In: *Three-dimensional kinematics of eye-, head-, and limb movements*, (Fetter, M., Tweed, D. and Misslisch, H., eds), Harwood Academic Publ., Amsterdam, pp. 33-42.
- [36] **Hess, B.J.M.** (1990) Dual-search coil for measuring three-dimensional eye movements in experimental animals. *Vision Res.* **30**: 597-602
- [37] **Hess, B.J.M., Van Opstal, A.J., Straumann, D. and Hepp, K.** (1992) Calibration of three-dimensional eye position using search coil signals in the rhesus monkey. *Vision Res.* **32**: 1647-1654

- [38] **Hering, E.** (1879) Die Raumsinn und die Bewegungen des Auges. In: *Handbuch der Physiologie*, (Vol. 3, pt. 1), (Hermann, L. and Vogel, F.C.W., eds), pp. 343-601, Leipzig
- [39] **Jürgens, R., Becker, W., and Kornhuber, H.H.** (1981) Natural and drug-induced variations of velocity and duration of human saccadic eye movements: evidence for a control of the neural pulse generator by local feedback. *Bil. Cybern.* **39**: 87-96
- [40] **Keller, E.L., Gandhi, N.J., and Shieh, J.M.** (1996) Endpoint accuracy in saccades interrupted by stimulation in the omnipause region in monkey. *Vis. Neurosci.* **13**: 1059-1067
- [41] **Legally, M.** (1928): *Vorlesungen über Vektor-Rechnung*. Akademische Verlagsgesellschaft, Leipzig.
- [42] **Mays, L.E., and Sparks, D.L.** (1980) Saccades are spatially, not retinocentrically, coded. *Science* **208**: 1163-1165
- [43] **Minken, A.W.H., Van Opstal, A.J. and Van Gisbergen, J.A.M.** (1993) Three-dimensional analysis of strongly curved saccades elicited by double-step stimuli. *Exp. Brain Res.* **93**: 521-533
- [44] **Minken, A.W.H., and Van Gisbergen, J.A.M.** (1994) A three-dimensional analysis of vergence eye movements at various levels of elevation. *Exp. Brain Res.* **101**: 331-345
- [45] **Mok, D., Ro, A., Cadera, W., Crawford, J.D., and Vilis, T.** (1992) Rotation of Listing's plane during vergence. *Vision Res.* **32**: 2055-2064
- [46] **Munoz, D.P., Waizman, D.M., and Wurtz, R.H.** (1995) Activity of neurons in monkey superior colliculus during interrupted saccades. *J. Neurophysiol.* **73**: 2313-2333
- [47] **Nakayama, K.** (1975) Coordination of extraocular muscles. In: *Basic mechanisms of ocular motility and their clinical implications*, (Lennerstrand, G. and Bach-y-Rita, P., eds), pp. 193-209, Pergamon Press, Oxford
- [48] **Nichols, M.J., and Sparks, D.L.** (1996) Component stretching during oblique stimulation-evoked saccades: the role of the superior colliculus. *J. Neurophysiol.* **76**: 582-600
- [49] **Robinson, D.A.** (1972) Eye movements evoked by collicular stimulation in the alert monkey. *Vision Res.* **12**: 1795-1808
- [50] **Robinson, D.A.** (1975) Oculomotor control signals. In: *Basic mechanisms of ocular motility and their clinical implications*, (Lennerstrand, G. and Bach-y-Rita, P., eds), pp. 337-374, Pergamon Press, Oxford.
- [51] **Roucoux, A., Guitton, D., and Crommelinck, M.** (1980) Stimulation of the superior colliculus of the alert cat. II. Eye and head movements evoked when the head is unrestrained. *Exp. Brain res.* **39**: 75-85
- [52] **Schnabolk, C. and Raphan, T.** (1994) Modelling three-dimensional velocity-to-position transformation in oculomotor control. *J. Neurophysiol.* **71**: 623-638
- [53] **Stanford, T.J., and Sparks, D.L.** (1994) Systematic errors for saccades to remembered targets: Evidence for a dissociation between saccade metrics and activity in the superior colliculus. *Vision Res.* **34**: 93-106
- [54] **Straumann, D., Zee, D.S., Solomon, D., Lasker, A.G. and Roberts, D.C.** (1995) Transient torsion during and after saccades. *Vision Res.* **35**: 3321-3334

- [55] Suzuki, Y., Büttner-Ennever, J.A., Straumann, D., Hepp, K., Hess, B.J.M. and Henn, V. (1995) Deficits in torsional and vertical rapid eye movements and shift of Listing's plane after uni- and bilateral lesions of the rostral interstitial nucleus of the medial longitudinal fasciculus. *Exp. Brain Res.* **106**: 215-232
- [56] Suzuki, Y., Hepp, K. and Henn, V. (1997) Three-dimensional eye movements evoked by electrical micro-stimulation of the trochlear nerve in alert rhesus monkeys. In: *Three-dimensional kinematics of eye-, head-, and limb movements*, (Fetter, M., Tweed, D. and Misslisch, H., eds), Harwood Academic Publ., Amsterdam, pp. 133-138.
- [57] Tung, W.-K. (1985) *Group Theory in Physics*. World Scientific Publishing Co., Singapore.
- [58] Tweed, D. (1997) Three-dimensional model of the human eye-head saccadic system. *J. Neurophysiol.* **77**: 654-666.
- [59] Tweed, D. (1997) Kinematic principles of three-dimensional gaze control. In: *Three-dimensional kinematics of eye-, head-, and limb movements*, (Fetter, M., Tweed, D. and Misslisch, H., eds), Harwood Academic Publ., Amsterdam, pp. 17-31.
- [60] Tweed, D.B. and Vilis, T. (1987) Implications of rotational kinematics for the oculomotor system in three dimensions. *J. Neurophysiol.* **58**: 832-849
- [61] Tweed, D.B. and Vilis, T. (1988) Rotation axes of saccades. *Ann. N.Y. Acad. Sci.* **545**: 128-139
- [62] Tweed, D.B. and Vilis, T. (1990) The superior colliculus and spatiotemporal translation in the saccadic system. *Neural Networks* **3**: 75-86
- [63] Tweed, D., Fetter, M., Andreadaki, S., König, E. and Dichgans, J. (1992) Three-dimensional properties of human pursuit eye movements. *Vision Res.* **32**: 1225-1238
- [64] Tweed, D., Misslisch, H. and Fetter, M. (1994) Testing models of the oculomotor velocity-to-position transformation. *J. Neurophysiol.* **72**: 1425-1429
- [65] Tweed, D., Glenn, B., and Vilis, T. (1995) Eye-head coordination during large gaze shifts. *J. Neurophysiol.* **73**: 766-779.
- [66] Van Gisbergen, J.A.M., Robinson, D.A. and Gielen, S. (1981) A quantitative analysis of generation of saccadic eye movements by burst neurons. *J. Neurophysiol.* **45**: 417-442
- [67] Van Gisbergen, J.A.M., Van Opstal, A.J., and Schoenmakers, J.J.M. (1985) Experimental test of two models for the generation of oblique saccades. *Exp. Brain Res.* **57**: 321-336
- [68] Van Opstal, A.J. (1993) Representation of eye position in three dimensions. In: *Multisensory control of movement*, (Berthoz, A., ed), pp. 27-41, Oxford University Press, Oxford
- [69] Van Opstal, A.J. and Hepp, K. (1995) A novel interpretation of the role of the SC in saccade generation *Biol. Cybern.* **73**: 431-445
- [70] Van Opstal, A.J., Hepp, K., Hess, B.J.M., Straumann, D. and Henn, V. (1991) Two-, rather than three-dimensional representation of saccades in monkey superior colliculus. *Science* **252**: 1313-1315

- [71] **Van Opstal, A.J., Hepp, K., Hess, B.J.M., Straumann, D. and Henn, V.** (1993) Experimental test of two models for the role of monkey superior colliculus in 3D saccade generation. In: *Multisensory control of movement*, (Berthoz, A., ed), pp. 240-254, Oxford University Press, Oxford
- [72] **Van Opstal, A.J., Hepp, K., Suzuki, Y. and Henn, V.** (1995) Influence of eye position on activity in monkey superior colliculus. *J. Neurophysiol.* **74**: 1593-1610.
- [73] **Van Opstal, A.J., Hepp, K., Suzuki, Y. and Henn, V.** (1996) Role of monkey nucleus reticularis tegmenti pontis in the stabilization of Listing's plane. *J. Neurosci.* **16**: 7284-7296.
- [74] **Van Opstal, A.J., Hepp, K., Suzuki, Y. and Henn, V.** (1997) Three-, rather than two-dimensional burst generation for spontaneous saccadic eye movements. In: *Three-dimensional kinematics of eye-, head-, and limb movements*, (Fetter, M., Tweed, D. and Misslisch, H., eds), Harwood Academic Publ., Amsterdam, 73-84.
- [75] **Vilis, T., Hepp, K., Schwarz, U. and Henn, V.** (1989) On the generation of vertical and torsional rapid eye movements in the monkey. *Exp. Brain Res.* **77**: 1-11
- [76] **Vilis, T.** (1997) Physiology of three-dimensional eye movements: saccades and vergence. In: *Three-dimensional kinematics of eye-, head-, and limb movements*, (Fetter, M., Tweed, D. and Misslisch, H., eds), Harwood Academic Publ., Amsterdam, 59-72.
- [77] **Westheimer, G.** (1957) Kinematics of the eye. *J. Opt. Soc. Am.* **47**: 967-974

APPENDIX A-1: Proof that quaternions describe rotations.

Without loss of generality, we choose a right-handed coordinate system such that the rotation axis, $\hat{\mathbf{n}}$, coincides with the $\hat{\mathbf{e}}_z$ axis, and the vector \mathbf{u} lies in the $(\hat{\mathbf{e}}_x, \hat{\mathbf{e}}_y)$ -plane, making an angle ϕ with the rotation axis. Thus, $\hat{\mathbf{n}} = (0, 0, 1)$, and the associated quaternions and vector are (from Eq. (17) and Eq. (18)):

$$\begin{aligned} q &= |q|(\cos(\theta) + \sin(\theta) \cdot k) \\ \mathbf{u} &= |u|(\cos(\phi) \cdot k + \sin(\phi) \cdot i) \\ q^{-1} &= |q|^{-1}(\cos(\theta) - \sin(\theta) \cdot k) \end{aligned} \quad (\text{A1})$$

By applying the rules defined in Eq. (14) it follows that

$$\begin{aligned} \mathbf{u}' = \mathbf{u}q^{-1} &= |u| \cos(\phi)(qkq^{-1}) + |u| \sin(\phi)(qiq^{-1}) \\ &= |u| \cdot (\cos(2\theta)i + \sin(2\theta)j) \\ &= R(\hat{\mathbf{e}}_z, 2\theta) \mathbf{u} \end{aligned} \quad (\text{A2})$$

which is indeed the vector, \mathbf{u} , rotated around axis $\hat{\mathbf{e}}_z$ (the invariant component under (A2), about an angle that is *twice* the quaternion angle θ).

Note, that the length of the quaternion does not play a role in describing the single-axis rotation. For this reason, it is customary to apply unit quaternions ($|q| = 1$).

APPENDIX A-2: Angular and coordinate velocity.

First, note that the quaternion product Eq. (15) obeys the following commutator relation:

$$pq - qp = 2 \mathbf{p} \times \mathbf{q} \quad (\text{A3})$$

which follows directly from Eq. (15). Second, we use the result of Appendix A-1, that the rotation of an initial vector, say \mathbf{s}_o , can be described by the quaternion product Eq. (19):

$$\mathbf{s}(t) = q(t)\mathbf{s}_o q^{-1}(t) \quad (\text{A4})$$

Then, the coordinate velocity vector is obtained by time differentiation of (A4):

$$\dot{\mathbf{s}}(t) = \dot{q}(t)\mathbf{s}_o q^{-1}(t) + q(t)\mathbf{s}_o \dot{q}^{-1}(t) \quad (\text{A5})$$

The right-hand factor of this equation may be evaluated as $\dot{q}^{-1} = -q^{-1}\dot{q}q^{-1}$, which follows from taking the time derivative of the definition $qq^{-1} = 1$. Then, the identity operator $q^{-1}q$ is used once more by substitution in the left-hand part of (A5). By using (A3) and (A4), this yields

$$\dot{\mathbf{s}}(t) = (\dot{q}q^{-1})\mathbf{s}(t) - \mathbf{s}(t)(\dot{q}q^{-1}) = 2V(\dot{q}q^{-1}) \times \mathbf{s}(t) \quad (\text{A6})$$

The scalar part of the quaternion $\dot{q}q^{-1}$, given by $S(\dot{q}q^{-1}) = \dot{q}_o q_o^{-1} + \dot{\mathbf{q}} \bullet \mathbf{q} = 0$. This follows from the fact that $S(\dot{q}q^{-1}) = d|q|^2/dt = 0$, because the quaternion length is fixed to 1.

So, to summarize

$$\dot{\mathbf{s}}(t) = (2\dot{q}q^{-1}) \times \mathbf{s}(t) \implies \boldsymbol{\omega}(t) = 2\dot{q}q^{-1} \quad \text{and} \quad \dot{q} = \frac{\boldsymbol{\omega}(t) \cdot \mathbf{q}}{2} \quad (\text{A7})$$

To obtain the equivalent relations for the rotation vector representation, we use the definition

$$\mathbf{q} = q_o \mathbf{r} \quad \text{and} \quad \dot{\mathbf{q}} = \dot{q}_o \mathbf{r} + q_o \dot{\mathbf{r}} \quad (\text{A8})$$

and, for unit quaternions Eq. (16):

$$q_o^2 = 1 - \mathbf{q} \bullet \mathbf{q} = \frac{1}{1 + \mathbf{r} \bullet \mathbf{r}} \quad (\text{A9})$$

Substituting (A8) and (A9) into Eq. (23), the result Eq. (28) is immediately obtained.

Similarly, substitution of (A8) into Eq. (22) yields:

$$\dot{q}_o \mathbf{r} + q_o \dot{\mathbf{r}} = \frac{q_o \boldsymbol{\omega} + \boldsymbol{\omega} \times q_o \mathbf{r}}{2} \quad (\text{A10})$$

Noting that $\dot{q}_o = -(\boldsymbol{\omega} \bullet \mathbf{q})/2$ and combining this with (A8) and (A10) yields Eq. (29).

APPENDIX A-3: The half-angle rule.

The torsional component of the angular velocity vector of the eye, for saccades in Listing's plane, is given by Eq. (28):

$$\omega_x = 2 \cdot (\mathbf{r}_y \cdot \dot{\mathbf{r}}_z - \mathbf{r}_z \cdot \dot{\mathbf{r}}_y) \quad (\text{A11})$$

Suppose that the eye initially looks down (angle ρ_y) and makes a leftward saccade (say with average velocity \bar{v}_z):

$$\mathbf{r} = \tan(\rho_y/2) \hat{\mathbf{e}}_y \quad \text{and} \quad \dot{\mathbf{r}} = \bar{v}_z \hat{\mathbf{e}}_z \quad (\text{A12})$$

It then follows that the angle, α , between $\boldsymbol{\omega}$ and the primary direction, $\mathbf{p} = \mathbf{r} \times \dot{\mathbf{r}}$, is given by

$$\cos(\alpha) = \frac{(\boldsymbol{\omega} \bullet \mathbf{p})}{|\boldsymbol{\omega}| \cdot |\mathbf{p}|} = \frac{\tan(\rho_y/2)}{|\hat{\mathbf{e}}_z + \tan(\rho_y/2) \hat{\mathbf{e}}_x|} = \sin(\rho_y/2) \Rightarrow \psi = 90 - \alpha = \rho/2 \quad (\text{A13})$$

Thus, when a saccade is made in a direction orthogonal to the eye position vector, the angle, ψ , between $\boldsymbol{\omega}$ en LP is given by $\rho_y/2$, which is *half* the eccentricity of initial eye position. This property is known as the '*half-angle rule*'.

Note, that in accordance with Listing's law, $\boldsymbol{\omega}$ can in principle tilt by any angle between $\{-\rho/2, +\rho/2\}$. For example, when \mathbf{r} and $\dot{\mathbf{r}}$ are parallel (e.g. the eye moves downward (or upward) from a downward fixation) the tilt angle ψ is zero. All eye movements that pass through the primary position have their angular velocity vector in LP.

APPENDIX A-4: Retinal error and motor error in 3D

The finite rotation formula Eq. (9) gives a straightforward recipe for calculating the orientation of a rotated body, once the rotation axis and angle are known.

Suppose that the eye is in the initial eye position, $\mathbf{r}_1 = \tan(\rho_1/2) \hat{\mathbf{n}} = R(\hat{\mathbf{n}}_1, \rho_1)$. Since the eye is in Listing's plane, the torsional component of \mathbf{r}_1 is zero, and the line of sight (which is eye fixed) points along $\hat{\mathbf{e}}_{1x}$.

A target at position \mathbf{r}_2 is foveated as soon as the new direction of the line of sight points at the target. This direction is given by the the gaze line in the new rotated eye-fixed coordinate system, $\hat{\mathbf{e}}_{2x}$.

The coordinates of the target, $\mathbf{s}_o = (s_{o,y}, s_{o,z})$ (i.e. the retinal error), with the eye in the initial position, \mathbf{r}_1 , are given by the projection of the future line of sight onto the current gaze direction, i.e.:

$$\begin{aligned} s_{o,y} &= (\hat{\mathbf{e}}_{2x} \bullet \hat{\mathbf{n}}_{1y}) \\ s_{o,z} &= (\hat{\mathbf{e}}_{2x} \bullet \hat{\mathbf{n}}_{1z}) \end{aligned} \quad (\text{A14})$$

When the eye fixates the new target, the gaze direction is described by a rotation vector: $\mathbf{r}_2 = R(\hat{\mathbf{n}}_2, \rho_2)$. By Listing's law Eq. (33), the position axes of both eye positions are in LP, so that they are perpendicular to the primary direction of the head-fixed primary Listing frame, $\hat{\mathbf{e}}_{ox}$:

$$(\hat{\mathbf{n}}_1 \bullet \hat{\mathbf{e}}_{ox}) = 0 \quad \text{and} \quad (\hat{\mathbf{n}}_2 \bullet \hat{\mathbf{e}}_{ox}) = 0 \quad (\text{A15})$$

We now express the retinal error in terms of the initial and final eye positions, by using the third-order Taylor approximation of the rotation formula Eq. (10), and the properties of vector triple-products: $\mathbf{a} \times (\mathbf{b} \times \mathbf{c}) = (\mathbf{a} \bullet \mathbf{c})\mathbf{b} - (\mathbf{a} \bullet \mathbf{b})\mathbf{c}$ and $\mathbf{a} \bullet (\mathbf{b} \times \mathbf{c}) = (\mathbf{a} \times \mathbf{b}) \bullet \mathbf{c}$.

Substitution into (A14) (only including terms up to $\mathcal{O}(\rho^3)$) yields (with $k=y, z$):

$$\begin{aligned} s_{o,k} &= (R_2(\hat{\mathbf{n}}_2, \rho_2)\hat{\mathbf{e}}_{ox} \bullet R_1(\hat{\mathbf{n}}_1, \rho_1)\hat{\mathbf{e}}_{ok}) \\ &= (\hat{\mathbf{e}}_{ox} + \rho_2 \hat{\mathbf{n}}_2 \times \hat{\mathbf{e}}_{ox} + \frac{1}{2}\rho_2^2 \hat{\mathbf{n}}_2 \times (\hat{\mathbf{n}}_2 \times \hat{\mathbf{e}}_{ox})) \bullet \\ &\quad (\hat{\mathbf{e}}_{ok} + \rho_1 \hat{\mathbf{n}}_1 \times \hat{\mathbf{e}}_{ok} + \frac{1}{2}\rho_1^2 \hat{\mathbf{n}}_1 \times (\hat{\mathbf{n}}_1 \times \hat{\mathbf{e}}_{ok})) \\ &= \rho_2 \hat{\mathbf{e}}_{ok} \bullet (\hat{\mathbf{n}}_2 \times \hat{\mathbf{e}}_{ox}) + \rho_1 \hat{\mathbf{e}}_{ox} \bullet (\hat{\mathbf{n}}_1 \times \hat{\mathbf{e}}_{ok}) \\ s_{o,y} &= (\rho_2 \hat{\mathbf{n}}_2 - \rho_1 \hat{\mathbf{n}}_1) \bullet \hat{\mathbf{e}}_{oz} = 2 \cdot \mathbf{d}_z \\ s_{o,z} &= (\rho_1 \hat{\mathbf{n}}_1 - \rho_2 \hat{\mathbf{n}}_2) \bullet \hat{\mathbf{e}}_{oy} = -2 \cdot \mathbf{d}_y \end{aligned} \quad (\text{A16})$$

Thus, in good approximation, retinal error is linearly related to the difference vector in Listing's plane between the final and initial eye positions. For eye positions within the periprimary range of 15 deg (the range within which the far majority of natural saccades is made), the approximation is better than 2.5%; but even up to 30° the error is of the same order than the natural scatter in saccade accuracy: 12% [30].